Surfaces and Interfaces 53 (2024) 105006

Contents lists available at ScienceDirect

Surfaces and Interfaces

journal homepage: www.sciencedirect.com/journal/surfaces-and-interfaces

Methyl Red-loaded halloysite nanotubes-based silica coatings for durable dyeing of polyester fabrics

Giulia Rando [a,1], Silvia Sfameni [a,1], Mariam Hadhri [b,1], Alessio Mezzi [c], Marco Brucale [d], Giovanna De Luca [e], Elpida Piperopoulos [f], Candida Milone [f], Dario Drommi [e], Giuseppe Rosace [b], Valentina Trovato [b,*], Maria Rosaria Plutino [a,*]

[a] Institute for the Study of Nanostructured Materials, ISMN–CNR, URT of Messina, c/o Department of ChiBioFarAm, University of Messina, Viale F. Stagno d'Alcontres 31, Vill. S. Agata, 98166 Messina, Italy
[b] Department of Engineering and Applied Sciences, University of Bergamo, Viale Marconi 5, 24044 Dalmine, Italy
[c] Institute for the Study of Nanostructured Materials, ISMN – CNR, via Salaria Km29.3, 00015, Monterotondo stazione, Rome, Italy
[d] Institute for the Study of Nanostructured Materials, ISMN – CNR, via P. Gobetti 101, 40129 Bologna, Italy
[e] Department of ChiBioFarAm, University of Messina, Viale F. Stagno d'Alcontres 31, Vill. S. Agata, 98166 Messina, Italy
[f] Department of Engineering, University of Messina, Contrada di Dio, S. Agata, 98166 Messina, Italy

ARTICLE INFO

Keywords:
Halloysite
Methyl red
Polyester fabrics
Sol-gel
(3-glycidyloxypropyl)trimethoxysilane
Dyeing coating

ABSTRACT

Since unmodified polyester fibres have no reactive groups like those in cellulose and protein fibres, they do not show an affinity for water-soluble acid, basic and direct dyestuffs. Only disperse dyestuff, a non-ionic dyestuff class with low molar mass molecules, proved to be useful for dyeing this man-made fibre following a solid–solid interaction; disperse dyestuffs do not form primary chemical bonds with polymer chains rather the dye colour is retained by H-bonds and Van der Waals forces. Herein, a new strategy for dyeing polyester fabrics with a direct dyestuff in a two-step strategy was designed and realized, using an organic–inorganic composite coating based on methyl red-loaded sol-gel modified halloysite nanotubes. In the first step two distinct reaction methods were compared to functionalize halloysite nanotubes with (3-Glycidyloxypropyl)trimethoxysilane, as a covalent crosslinker between the halloysite nanotubes and fibres, (i) in water and (ii) in ethanol, using $BF_3O(C_2H_5)$ and chloridric acid (HCl) as catalysts, respectively.

In the second step, methyl red loaded GPTMS modified halloysite sols were applied onto polyester fabrics by impregnation. The amount of methyl red dyestuff was evaluated to be superior for the complex realized in ethanol than in water, thus promoting homogeneous nanocomposite coatings on treated polyester samples. Methyl red loaded sol-gel modified halloysite complex, as well as treated and untreated samples, were investigated to characterize their properties and morphology. NMR investigation confirmed the structure of the new complex, validating the successful dyestuff coordination reaction at GPTMS.

The influence of treatments on the morphology of fibres surfaces was demonstrated by Scanning Electron Microscopy (SEM), Energy Dispersive X-ray spectroscopy (EDX), and Atomic Force Microscopy (AFM) analyses, highlighting the influence of GPTMS-based composites on the microstructure of functionalized polyester fibres. To further confirm if the suggested approach offers a stable dyestuff loading on PE, diffuse reflectance spectroscopic studies, X-ray Photoelectron Spectroscopy (XPS) and colour fastness to rubbing and washing tests were carried out on the coated polyester.

All findings make sol-gel based modification of halloysite a reliable and promising method for eco-friendly dyeing processes of polyester fabrics.

Abbreviations: HNT, halloysite nanotubes; GPTMS, (3-glycidyloxypropyl)trimethoxysilane; MR, methyl red; PE, polyethylene terephthalate or polyester (synonym).

* Corresponding author.
[1] These authors equally contribute to the paper.

https://doi.org/10.1016/j.surfin.2024.105006
Received 21 May 2024; Received in revised form 20 August 2024; Accepted 23 August 2024
Available online 24 August 2024

1. Introduction

In recent years, there has been a growing research interest in hybrid organic inorganic materials, based on inorganic fillers and sol-gel techniques, for treating and affording functional textiles. These products are viewed as beneficial substitutes for the harmful chemicals traditionally used in textile coating and finishing processes [1]. The design and development of new products and methods for treating textile fabric surfaces generate significant interest from various scientific fields, with intriguing applications extending from basic study to practical application [2].

In this scenario, because of their typical mesoporous structure and excellent chemical and thermal stability, in recent years naturally occurring one-dimensional tubular nanomaterials have received a lot of attention, and they were also successfully employed as filler for macromolecules (polymers and resins) in order to obtain nanomaterials for drug delivery [3,4], catalysis [5–7], nanocomposites [8,9], azo-dye [6, 10] and wastewater treatment [11,12] applications. These materials include natural layered aluminosilicates [13] like halloysite nanotubes (HNTs), natural one-dimensional nanomaterials that can be found in some soil in wet tropical and subtropical regions, weathered rocks, and soil generated from volcanic ashes [14]. HNTs exist in two different forms, namely dehydrated ($Al_2Si_2O_5(OH)_4$: basal distance of 7 Å) and hydrated halloysite ($Al_2Si_2O_5(OH)_4 \cdot nH_2O$: basal distance of 10 Å) consisting of nanotubes/nanoscrolls, even if other forms such as the platy and pseudo-spherical shapes have also been reported [15]. Halloysite is characterized by a 1:1 ratio of silicon-oxygen tetrahedral layers to aluminium–oxygen octahedral layers that undergo different forces in the formation process (i.e. halloysite sheets curl in the direction of the Al–O octahedral layer), thus resulting in the characteristic halloysite tubular shape [6].

Halloysite usually has an internal diameter of roughly 1–30 nm and an external diameter of 30–70 nm, making this one-dimensional material suitable for capturing and subsequent controlled release of guest molecules [16–18]. The formation of the curled crystals stems from the mismatch between the octahedral gibbsite-like sheet and the silica-like sheet, resulting in the exposure of Si–O groups on the external surface, Al–OH groups on the internal surface, and Al–OH and Si–OH groups along the material's edges (see Fig. 1) [19,20], which provide suitable reaction sites for modification and functionalization of HNTs [21–23]. The immobilization of molecules in halloysite nanotubes can be performed both inside and outside of the tubes. It can permit materials to be treated with non-specific chemicals, prevent molecule aggregation, reduce the cost of processes, and enhance the chemical and thermal, as well as mechanical properties of treated samples. The empty tube, featuring a pre-defined diameter, allows the entrance of molecules with specific sizes, thus giving shape selectivity to the immobilization. Regioselectivity can also be achieved when only part of the molecule penetrates the tube and comes in contact with the active site [14].

Compared with other nanotubes such as CNTs, halloysite nanotubes, which have a crystal structure close to CNTs, offer exciting qualities such as cheap cost, environmental friendliness, and tons availability, as well as a high aspect ratio (length/diameter) (ranging from 8 to 50) that promotes filler-polymer interaction [24]. When HNTs are introduced into a polymeric matrix, the physiochemical characteristics of the polymer improve, resulting in improved thermal and mechanical performance [25]; therefore, several nanocomposites have been obtained using HNT as filler for different kinds of polymeric matrices [26,27].

Due to the higher length-diameter ratio, lower hydroxyl density and higher distribution of charge on the outer surface, as well as weaker hydroxyl hydrogen bonding, HNTs are more likely to be homogeneously dispersed in polymer matrices, than other conventional nanotubes [28]. For example, they have commonly been functionalized with organosilane compounds of the type R–SiX_3, where R is a non-hyrolyzable and reactive functional group such as an amine group, thiol or epoxy group, while X is a hydrolysable group, including methoxy, ethoxy and trimethylsiloxy, etc. Due to their special structure, the silane precursors have a reactive group able to chemically bond with an inorganic material (silica, iron oxide, etc.), meanwhile they have a functional group capable of chemically reacting with an organic molecule (organic small molecules or polymers) [29]. In this way, the organosilane agent and the hydroxyl groups in the surface structure of HNTs can be covalently bonded, thus allowing a fine tuning of the surface of the clays and, in the case of HNTs hosting immobilized molecules, enhancing their reactivity and preventing their leaching [30,31].

These nanofiller-containing composite coatings can be used to functionalize textile fibres, in order to meet the demands of production with high added value but low environmental impact [32]. Lvov et al., for example, developed a clay nanotube coating on cotton fibres for enhanced flame-retardancy and antibacterial properties. In particular, they loaded halloysite nanotubes with colour-enhancing dyes, antimicrobial chloramphenicol or silver, providing architectural

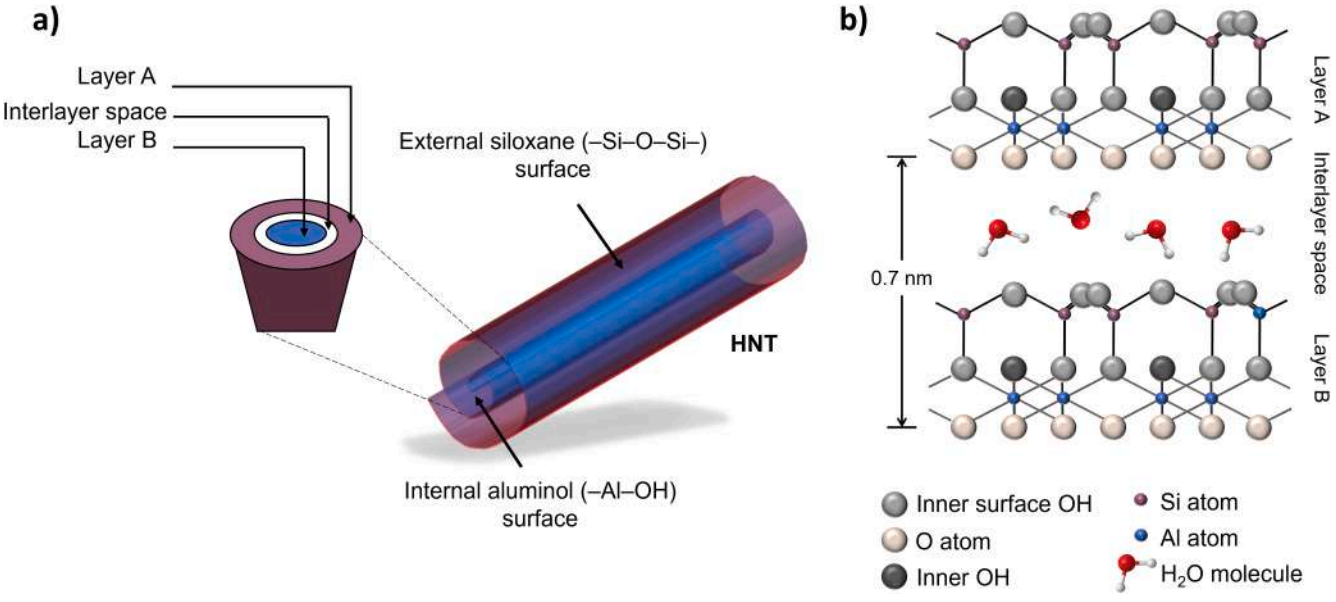

Fig. 1. HNT interlayed structure (a) with detailed composition (b).

organic/inorganic coatings with complex functionality on raw cotton [33]. Halloysite was also bound onto commercial cotton fibres by the employment of biopolymer alginate with Ca^{2+} crosslinking, for robust and high-performance hemostatic dressing [34].

Among all synthetic fibres, polyethylene terephthalate (PE) is a man-made fibre composed of linear polymers comprising, for at least 85 % by mass, ester compounds derived from benzene-1,4-dicarboxylic acid (terephthalic acid) and diol, arranged in linear macromolecular chains. PE is typically manufactured using terephthalic acid or dimethyl terephthalate in conjunction with ethylene glycol. It is the clear market leader, making up over half of the global textile fibres due to its exceptional mechanical and physical properties, high strength, stiffness, resistance to wear and wrinkles, adaptability, and reasonably cheap cost [35]. Nevertheless, because of their high crystallinity, density, hydrophobicity, and absence of chemically reactive groups, polyester fabrics have several drawbacks, including low moisture retention and challenges in dyeing processes, demanding substantial energy for water dyeing and use of carriers to facilitate the adsorption of disperse dyestuffs [36]. In many studies, polyester underwent modification through either chemical hydrolysis or irradiation to introduce functional groups onto its surface, enhancing the polymer's hydrophilicity before dyeing, including microwave irradiation or plasma treatments [37,38]. Since polyester fibres typically have a very compact structure and high crystallinity, which can resist dyestuff uptake, the choice of dyes for them is limited to the dispersed dye range. The dyed polyester should be cleared of surface-deposited dyestuff and auxiliaries through treatment with detergent or by reductive or oxidative treatments to secure optimum dyeing fastness [39]. Low fastnesses to perspiration or water in polyester are always associated with loose dyestuff particles on the fibre surface [40].

To overcome these drawbacks and to avoid such pretreatments of polyester fabrics, a new strategy for dyeing PE with 2-(4-dimethylaminophenylazo)benzoic acid (methyl red, MR), selected as a representative molecule of azo dyestuffs, was developed in this study. Azo dyestuffs are widely utilized in industry because of their versatile applications in several sectors, such as textile dyeing [41], dye-sensitized solar cells (DSSC), metallochromic indicators, optical sensors [42] and photosensitizers [43].

The possibility of dyeing polyester samples with azo dyestuffs entails the following advantages compared with dispersed ones: (i) shades are more brilliant; (ii) dyestuffs are cheaper; and (iii) sublimation fastness of the dyestuffs is high.

With this aim, trimethoxy-[3-(oxiran-2-ylmethoxy)propyl]silane (GPTMS) precursor bearing methoxysilyl groups and an epoxy ring was selected as a coupling agent, exploiting its possibility to immobilize MR-loaded halloysite nanotubes (through the reactive epoxy function) onto the polyester surface (through hydrolysed Si–OH groups) [44,45]. Indeed, GPTMS is mostly employed since it undergoes a ring-opening reaction with the epoxy groups reacting with the carboxyl groups present in the MR structure, to form an ester group. Moreover, after undergoing hydrolysis, siloxane groups participated in co-condensation reactions and with hydroxyl and/or carboxyl groups located at the end of the polyethylene terephthalate polymer chains. These groups present on the surface of the polyester enabled the establishment of covalent bonds between fibres and hybrid segments possessing a siloxane backbone connected to dyestuffs-loaded halloysite nanotubes, offering tuneable thickness, porosity, optical transparency, and biocompatibility [46].

Therefore, methyl red-loaded GPTMS functionalized halloysite nanotubes were fabricated by blending HNTs to GPTMS-based (either modified with MR adduct) polymer matrices, and thus characterized by different chemical-physical techniques. NMR spectroscopy was employed to characterize and quantify the extent of the proposed reaction in terms of surface morphology and chemical structure. The chemical composition of xerogels coated onto polyester fabrics was characterized through ATR FT-IR spectroscopy. Changes in the morphology of treated polyester fabrics were characterized with scanning electron microscopy (SEM), equipped with an energy dispersive X-ray spectroscopy (EDX), and atomic force (AFM) microscopy. In addition, diffuse reflectance spectroscopy measurements were performed on the developed polyester fabrics to verify whether the proposed pad-cure based method provides a stable dyestuff loading on PE. Then, the surface chemical composition was investigated by X-ray Photoelectron Spectroscopy (XPS). Finally, the dyed silica-containing fabrics colour strength and fastness to rubbing and washing properties were evaluated. The effectiveness of this innovative and successful dyeing process of PE samples was thoroughly discussed based on the overall experimental findings.

From a sustainability perspective, relative to exhaust dyeing, the proposed padding-based method offers many advantages [47]:

- lower liquor-to-fibre ratio in the dyebath;
- lower amounts of leftover dyebath solution;
- faster dye application;
- easier control of dye levelness on the fabric;
- no electrolyte required for exhaustion.

2. Experimental details

2.1. Materials and methods

The employed chemical reagents (3-glycidoxypropyltrimethoxysilane, GPTMS; methyl red, MR; boron trifluoride; halloysite nanotubes, HNTs; hydrochloric acid) and the solvents (absolute ethyl alcohol and CHROMASOLV® water for HPLC) were purchased from Sigma Aldrich Co at the highest purity available and used as received. Methanol-d_4 (99.9 atom% D) used for the NMR spectra was purchased from Sigma Aldrich Co and used as received, without further purification.

100 % pure polyester fabrics (PE, with mass per unit area 140 g/m^2) were used, previously washed to eliminate any impurities of natural or synthetic origin, in a water solution containing 2 % non-ionic detergent (BERDET WF, detergent, kindly supplied by Europizzi, Urgnano (BG), Italy), at pH 7 and under a temperature of 40 °C for about 20 min. Washed samples were then rinsed differently times with deionized water, dried and stored at atmospheric pressure under a temperature of 20 ± 2 °C and humidity of 65 ± 4 %, before carrying out any experiments.

2.2. Synthesis of HNT_GPTMS sol

Method in ethanol solution (HNT_GPTMS@Et)

HNT (0.205 g, 0.70 mmol) was slowly dispersed in a round bottom flask containing 200 mL of ethanol, and the resulting mixture was stirred and heated at 70 °C (under reflux conditions) for 1 h. GPTMS (7 g, 29.6 mmol) and HCl 0.1 M (catalytic amount: 2 mL) were added dropwise in this order, and the obtained mixture was left to react under stirring at 70 °C for 24 h. After this time, the pH of the mixture was adjusted above 5 using NaOH (0.1 M). The insoluble residue of HNT was removed through filtration with Millipore® filter, obtaining a transparent hybrid sol (HNT_GPTMS@Et sol).

Method in water solution (HNT_GPTMS@W)

Similar to the previous procedure, HNT (0.2 g, 0.34 mmol) was dispersed in a round bottom flask containing 200 mL of deionized water and the resulting mixture was stirred and heated at 70 °C for 1 h. GPTMS (7 g, 29.6 mmol) was slowly added to the resulting mixture, and thus, 10 mL of a $BF_3O(C_2H_5)_2$ solution (0.35 g, 2.47 mmol, 50 mL) was added. After 24 h from the first addition of the catalyst, the resulting mixture (whose pH was corrected above 5 with NaOH 0.1 M) was filtered from the insoluble HNT residue with a Millipore® filter, obtaining a transparent sol (HNT_GPTMS@W).

2.3. Functionalization of HNT_GPTMS sol with MR dyestuff

In the next steps, the functionalization of both hybrid sols with a dyestuff, was realized using Methyl Red. In a flask containing 100 mL of HNT_GPTMS@Et sol (or HNT_GPTMS@W sol), MR (0.095 g, 0.35 mmol) was added under vigorous stirring. The obtained mixture was heated for 15 min, obtaining in the end the HNT_GPTMS_MR@Et and HNT_GPTMS_MR@W sols. Following the production of the sols, the next step was to impregnate the fabrics.

The purity of the starting materials and the characterization of the reaction products as obtained in ethanol were determined using ^{1}H NMR assignment.

3-glycidoxypropyltrimethoxysilane (GPTMS), ^{1}H NMR (500 MHz, methanol-d_4, 298 K) δ: 3.73 (dd, $^3J_{gem}$ = 11.6 Hz, $^4J_{HH}$ = 2.8 Hz 1H, H_{4a}), 3.55 (s, br, 9H, 3 × OCH_3), 3.46 (td, $^3J_{HH}$ = 6.6, 4.4 Hz, 2H, H_3), 3.30 (dd, $^2J_{gem}$ = 11.4 Hz, $^3J_{HH}$ = 6.3 Hz, 1H, H_{4b}), 3.11 (ddt, $^3J_{HH}$ = 6.2, 4.2 Hz, $^4J_{HH}$ =2.7 Hz, 1H, H_5), 2.76 (dd, $^3J_{HH}$ = 5.1, 4.2 Hz, 1H, H_{6a}), 2.57 (dd, $^3J_{HH}$ = 5.1, $^4J_{HH}$ =2.7 Hz, 1H, H_{6b}), 1.65 (m, 2H, H_2), 0.66 (m, 2H, H_1).

4-Dimethylaminoazobenzene-21-carboxylic acid (MR). ^{1}H NMR (500 MHz, methanol-d_4, 298 K) δ: 8.02 (d, $^3J_{HH}$ = 7.9 Hz, 1H, $H_{3'}$), 7.89 (d, $^3J_{HH}$ = 7.9 Hz, 1H, $H_{6'}$), 7.82 (d, $^3J_{HH}$ = 9.2 Hz, 2H, $H_{2,6}$), 7.72 (dd, $^3J_{HH}$ = 7.9 Hz, 1H, $H_{5'}$), 7.59 (dd, $^3J_{HH}$ = 7.9 Hz, 1H, $H_{4'}$), 6.96 (d, $^3J_{HH}$ = 9.2 Hz, 2H, $H_{3,5}$), 3.22 (s, 6H, N—CH_3).

4-Dimethylaminoazobenzene-21-carboxylic acid, GPTMS ester (GPTMS_MR). ^{1}H NMR (500 MHz, methanol-d_4, 298 K) δ: 8.17 (d, $^3J_{HH}$ = 7.9 Hz, 1H, $H_{3'}$), 8.11 (d, $^3J_{HH}$ = 7.9 Hz, 1H, $H_{6'}$), 7.88 (d, $^3J_{HH}$ = 9.2 Hz, 2H, $H_{2,6}$), 7.76 (dd, $^3J_{HH}$ = 7.9 Hz, 1H, $H_{5'}$), 7.43 (dd, $^3J_{HH}$ = 7.9 Hz, 1H, $H_{4'}$), 7.36 (d, $^3J_{HH}$ = 9.2 Hz, 2H, $H_{3,5}$), 3.91 (m, br,1H, $H_{5''}$), 3.65 (m, br, 2H, $H_{6''}$), 3.58 (m, br, buried under other signals, $H_{4''}$), 3.46 (m, br, buried under other signals, 2H, $H_{3''}$), 3.33 (s, 6H, N–CH_3), 1.71 (m, br, 2H, $H_{2''}$), 0.69 (m, br, 2H, $H_{1''}$).

4-Dimethylaminoazobenzene-21-carboxylic acid, GPTMS ester (HNT_GPTMS_MR). ^{1}H NMR. (500 MHz, methanol-d_4, 298 K) δ: 7.83 (d, $^3J_{HH}$ = 9 Hz, 2H, $H_{2,6}$), 7.63 (d, br, $^3J_{HH}$ = 8 Hz, 1H, $H_{6'}$), 7.51 (m, br, 1H, $H_{3'}$), 7.36 (m, br,1H, $H_{5',4'}$), 6.86 (d, $^3J_{HH}$ = 9 Hz, 2H, $H_{3,5}$), 3.80 (m, br, 2H, $H_{5''}$), 3.60 (m, br, buried under other signals, 2H, $H_{6''}$), 3.47 (m, br, buried under other signals, 2H, $H_{3'',4''}$), 3.02 (s, 6H, N—CH_3), 1.67 (m, br, 2H, $H_{2''}$), 0.68 (m, br, 2H, $H_{1''}$).

2.4. Sol–gel treatment of the polyester fabrics

In this study, both MR-loaded functionalized HNTs-containing solutions, i.e. HNT_GPTMS_MR@Et and HNT_GPTMS_MR@W sols, prepared according to previously described procedures, and the corresponding MR solutions, were used for dyeing PE fabrics (20 cm × 30 cm) by simple pad dry-cure method using a two-roll laboratory padder (Werner Mathis, Zurich, Switzerland) by setting up a nip pressure of 3 bar. After impregnation, the wet-treated polyester fabrics were dried (80 °C, 5 min) and cured (210 °C, 3 min) in a convection oven. The obtained textiles were coded as PE-MR and PE-GPTMS_MR, both @Et and @W, respectively.

Finally, treated samples were washed repeatedly (detergent 1 % by weight, 1 and 5 wash cycles) to test the resistance of the fabric coating to washing and to eliminate excess dyestuff, if present, dried and stored under standard conditions in an environmental chamber. As a point of comparison, the corresponding fabrics are prepared by application of the sol in the absence of dyestuff.

To evaluate the washing resistance of each coating, samples were washed with 1 and 5 washing cycles with a Labomat Mathis equipment (Werner Mathis AG) according to the international standard EN ISO 6330:2000.

The total dry amount of coating (A, wt%) on polyester fabrics was measured through Eq. (1) using a Mettler balance (10^{-4} g):

$$A = \frac{W_2 - W_1}{W_1} \times 100 \quad (1)$$

where W_1 and W_2 are the PE fabric weights before and after the impregnation step, respectively. In the same way, the weight loss percentage (WLW, wt%) of dyed polyester fabrics was measured after 1 and 5 washing cycles, using the same Eq. (1), where W_1 and W_2 are the weight of treated samples before and after washing cycles, respectively. Both A% and WLW% for each polyester treatment are summarized in Table 1.

2.5. Characterization and functional properties of treated fabrics

Nuclear Magnetic Resonance Spectroscopy (NMR). All NMR measurements were performed in methanol-d_4 at 298.2 (± 0.1) K. The ^{1}H NMR spectra were obtained with a Varian 500 spectrometer, equipped with a 5 mm OneNMR (TM) operating at 500.1. All chemical shifts are reported in parts per million (ppm), at low fields compared to tetramethylsilane (Me_4Si) as internal standard (δ = 0.0 ppm), or referred to the remaining protiated methanol-d_4 solvent signal (δ = 3.30 ppm). The coupling constants, J, are given in Hertz. The purity of all the starting materials and the reaction products obtained in ethanol were determined by ^{1}H NMR spectroscopy, and in any case clean spectra were obtained with the correct integration. NMR resonances were assigned with the help of two-dimensional homonuclear (gCOSY) experiments.

Attenuated total reflection FT-IR Spectroscopy (ATR FT-IR). Fourier transform infrared analysis (ATR FT-IR) was performed on the dry powders obtained in ethanol using a V-6600 Jasco Spectrometer, including the intuitive Spectra Manager™ Suite with integrated search software solution, KnowItAll® Informatics and database JASCO Edition (JASCO Europe s.r.l., Cremella, LC, Italy), endowed with an attenuated total reflection (ATR) accessory. Spectra were recorded at room temperature in the 4000–500 cm^{-1} range.

Scanning Electron Microscopy (SEM) Analysis. The two-dimensional morphology and structure of the surface fibres of the original and treated polyester fabrics with ethanolic sols, together with the EDX mapping, were obtained using a Scanning Electron Microscopy (SEM) (FEI Quanta FEG 450, Thermo Fisher Scientific, Hillsboro, Oregon, USA). A low vacuum voltage of 5 kV was used in any case. Energy Dispersive X-ray Spectrometry (EDS) and EDS mapping were performed at 20 kV, still in low vacuum. All the samples were placed on aluminum supports by means of a carbon graphite adhesive prior to testing.

Atomic Force Microscopy. AFM imaging was performed in PeakForce mode with ScanAsyst-Air probes (Bruker, USA) on a Multimode 8 microscope (Bruker, USA) equipped with a Nanoscope V controller and a type JV piezoelectric actuator. Textile samples treated with ethanolic sols were fixed to sample pucks via double-sided adhesive tape and scanned in air at room temperature. Background subtraction and image analysis were performed on Gwyddion 2.61 open-source software [48].

UV–Vis Spectroscopy. The UV-absorption spectra were recorded using a UV/vis spectrophotometer equipped with a halogen lamp (5 W) and a reflection probe (mod. QR600–7-SR-125F). This latter consists of a fibre optic Y-cable with a 6-around-1 fibre bundle design, the 6-fibre leg connected to the light source, and the single-fibre leg to the spectrometer. Reflectance spectra were recorded with the probe perpendicular to the sample's surface and relative to a PTFE standard with 1 s integration times, an average of 10 acquisitions, and a boxcar smoothing of 2.

The suspensions of nanomaterials, functionalized with GPTMS, were purified by centrifugation with the Hermle Labortechnik High-speed centrifuge, in 50 mL tubes, with a speed of 30,000 rpm. Diffuse reflectance measurements were recorded with an Ocean Optics mod. S2000.

Powder X-Ray Diffraction (XRD). The intercalation and the basal spacing study of the clay was carried out by using a D8 Advance Bruker instrument (Bruker, Billerica, MA, USA) equipped with a monochromatic CuKα radiation source (40 kV, 40 mA). Bragg-Brentano theta-

Table 1
Add-on, weight loss after 1 and 5 washing cycle percentage of coated samples with HNT_GPTMS and HNT_GPTMS_MR sols both in ethanol and water solutions.

Sample	A (%)	WLW (%) after 1 washing cycle	WLW (%) after 5 washing cycles
PE-HNT_GPTMS@Et	1.73 %	0.04 %	0.09 %
PE-HNT_GPTMS_MR@Et	2.07 %	0.28 %	0.27 %
PE-HNT_GPTMS@W	1.55 %	0.07 %	0.07 %
PE-HNT_GPTMS_MR@W	1.69 %	0.65 %	0.17 %

2theta configuration and a scanning speed of 0.1°/s were used to examine the samples obtained in ethanol in a wide range, from 10° to 80°

XPS Spectroscopy. The surface chemical composition of both untreated and treated fabrics with ethanolic sols was investigated by X-ray Photoelectron Spectroscopy (XPS), using an ESCALAB MkII (VG Scientific, East Grinstead, UK) spectrometer, equipped with a non-monochromatized Al Kα source and a five channeltrons detection system. The samples were fixed to the holder by a metallic clip. The spectra were collected at 40 eV pass energy and the binding energy scale was calibrated positioning the C 1 s peak from adventitious carbon at BE = 285.0 eV. All data were collected and processed by Thermo Avantage v.5 software.

Fastness to washing. To test laundering durability, the dyed samples underwent up to five washing cycles according to a modified ISO 105C10:2006 standard method. The test was performed at 40 °C for 30 min, using 400 mL capacity sealed stainless-steel pots in a laboratory-scale Mathis Labomat machine (Werner Mathis, Zurich, Switzerland), with 5 mg/l standard non-phosphate detergent without optical brighteners. After washing, the samples were rinsed with distilled water (pH= 5.5) and then dried at room temperature on a flat surface. Colour evaluation of the dyed samples was performed by a double beam UV–Vis scanning spectrophotometer (Thermo Nicolet Evolution UV–Vis 500), equipped with diffuse reflectance accessory (RSA-PE150 Labsphere), under illuminant D65 and using a 10° standard observer. Reflectance spectra were collected in the spectral region between 380 nm and 770 nm with 10 nm intervals.

The colour difference magnitude was quantified using the measured values of CIE L*a*b coordinates, where L*, a*, and b* define lightness-darkness, red/green, and yellow/blue values, respectively. Similarly, ΔL*, Δa*, and Δb* indicate the difference of each value compared to the dyed fabric, setting the unwashed sample as a standard and the washed dyed fabrics as the samples, according to Eq. (2):

$$\Delta E^{*} = \sqrt{(\Delta L^{*})^{2} + (\Delta a^{*})^{2} + (\Delta b^{*})^{2}} \tag{2}$$

where ΔL* is the lightness difference, Δa* and Δb* are the differences in a* and b* values. Chroma (C*) is the strength or dominance of the hue and it can be described as a saturation of a colour.

The colour data was the average of three different places on the sample, and the colour yield (K S^{-1}) value was calculated by using the following Kubelka-Munk (Eq. (3)):

$$\frac{K}{S} = \frac{(1-R^{2})}{2R} \tag{3}$$

where R is the reflectance of the dyed cotton fibre sample at the λ_{max} absorption and K and S are the absorption and scattering coefficients, respectively.

According to Pei et al. [49], the level dyeing property (Sγ(λ)), corresponding to the standard deviation of K S^{-1} values at 12 different randomly selected points [50], was determined by employing the Eq. (4):

$$S\gamma(\lambda) = \sqrt{\frac{\sum_{i=1}^{n}\left[\frac{\left(\frac{K}{S}\right)_{i\lambda}}{\left(\frac{K}{S}\right)_{i\lambda}} - 1\right]^{2}}{n-1}} \tag{4}$$

The colour change significance was evaluated concerning the human eye perception threshold, according to the confirmed range of colour change perceptibility [51]. Then, ΔE* values ranging from 0.0 to 1.0 were considered as not perceptible (below the threshold of 0.7, colours can be considered almost identical), between 1.1 and 3.0 as visually perceptible, while results higher than 3.1 were considered as clearly visible. For each experiment, an average value was determined based on three measured data, with a standard deviation always below 5 %.

Fastness to rubbing. Dry and wet colour fastness to rubbing were examined using an Atlas CM-5 Tester, according to AATCC 8–2005 test (Colourfastness to Crocking), technically equivalent to ISO 105-X16:2016. The dyed sample was placed on the base of the rubbing tester (also named "crock meter") so that it rested flat on the abrasive cloth with its long dimension in the direction of rubbing. A square of white testing fabric (5 cm × 5 cm) was forced to slide on the tested sample back and forth 20 times by turning the crank 10 complete turns. The control cotton cloth is then compared to a rating scale of pairs of standard grey (ISO 105-A02) from 1 (worst performing, indicating the highest level of colour transfer) to 5 (best performing, the lowest level of colour transfer) under appropriate lighting conditions for the evaluation of the staining. For the wet rubbing test, the control test square was thoroughly wetted in ultrapure water. The rest of the procedure was the same as the dry test. Also in wet conditions, the staining on the white crocking cloth was assessed using the grey scale.

3. Results and discussions

3.1. HNTs functionalization

Halloysite nanotubes were functionalized by reaction with a proper silane precursor by means of sol-gel technique, a very simple synthetic method which allows the formation of a 3D-porous silane-based network. The silane precursor, typically a $Si(OR)_n$ alkoxide or a functional derivative of general formula $SiR_x(OR)_{n-x}$, may crosslink by hydrolysis and condensation reactions, [52,53] or either incorporate functional organic molecules or nanofillers into this solid matrix, giving rise to functionalized hybrid sol-gel and xerogel of high thermal and mechanical stability [54].

GPTMS is certainly one of the most widely used and versatile organic silanes for manufacturing hybrid materials. In particular, the synthesis of hybrid materials based on the epoxy molecule GPTMS is a multi-step process, which includes the formation of a silane-based 3D matrix and the functionalization of the epoxide, by epoxy ring opening that can be then used in the functionality of organic molecules [55,56]. Several variables are strictly interdependent with the final result obtained and with the yield of the process, including the solvent, the quantity of water, the used catalyst, the temperature and the pH value. In the presence of a nucleophile agent, such as a chromophore or an appropriately structured nanomaterial, an addition to the GPTMS silane epoxide precursor through an epoxy ring-opening reaction can be

observed, promoting the formation of an inorganic-organic silane network [57].

To create sol-gel matrices incorporating nanofillers of organic or inorganic origin, such as halloysite, to enhance the physicochemical properties and mechanical characteristics of the sol-gel coated fabric fibres, we opted to modify an existing sol-gel synthetic approach based on GPTMS, which had previously been used for successful dyestuff applications on cotton [58]. The common feature of halloysite nanotubes, aluminosilicate-based nanofillers, is that they present external and internal –OH groups, together with interlayered water molecules. Therefore, the use of the GPTMS is particularly suitable. In fact, it can bind, by condensation, to nanofillers using its methoxysilane end and the –OH group, leading to the loss of CH_3OH. Additionally, GPTMS possesses an available epoxy group that, in the presence of a suitable catalyst, can undergo nucleophilic attack by chromophores, or other molecules in a solution featuring opportune charged or nucleophilic groups ($–COO^-$, $–SO_3^-$, $–NH_2$), giving rise through the epoxy-ring reaction to the formation of a new adduct featuring the hydrolyzed OH– functionality and the bound substituent nucleophilic molecule [59].

In this work, two different reaction approaches were used for the synthesis of the GPTMS-based hybrid containing HNT as nanofiller (Fig. 2): (i) in water with $BF_3O(C_2H_5)$ as catalyst; (ii) in ethanol using traces of acid (HCl) as catalyst. Various procedures were carried out to optimize the best synthetic experimental conditions (i.e. varying solvents, volumes, and catalyst/ nanomaterial/GPTMS concentrations) leading to the best performing homogeneous sols.

To avoid the formation of undesidered insoluble material, a dilution of the catalyst was carried out. In this regard, in the aqueous or ethanolic solutions, the pre-established catalyst additions (BF_3 or HCl) were carried out little by little, to slow down the reaction between GPTMS and HNTs. In the case of ethanolic solutions it was chosen to use a reflux temperature ($T = 70\ °C$) to activate the siloxanes of the GPTMS. In any case, the pH of the solution was brought back to a neutral value, at the end of the reaction, to stop the reaction itself. The solution was finally filtered with a Millipore® filter, to eliminate the insoluble component.

Once both protocols were set up, the same reaction was carried out in the presence of the Methyl Red (MR) dyestuffs, with the intent of adsorbing the dyestuff on the surface or in the cavities of the used nanostructures, to apply the chromophore, linked via hydrolyzed and open-ring GPTMS or either directly coordinated to the nanofiller, more effectively on the fabric.

While the surface charges remain unaffected with varying pH, the charges at the edges are attributed to the protonation/deprotonation of silanol and aluminol groups, which are pH-dependent [60]. In the present study, methyl red immobilization was accomplished in both water (pH between 5 and 6) and organic solvents (ethanol), which hindered the determination of solution pH. In the case of the MR, the aluminol groups, situated on the inner side of the nanotube or at the tube ends, were identified as their preferred immobilization sites on the support. Indeed, in the pH range of 5 to 6, these sites undergo protonation and exhibit a positive charge: $Al(OH_2)^+$. Bearing in mind that the isoelectric point of halloysite is around pH 3.0, the silanol groups at the edge must be deprotonated entirely at pH higher than 3, SiO^- being the predominant species in the product [14].

Fig. 3 shows the reaction schemes for the functionalization of the siloxane-based external or aluminate-based surface of the halloysite nanotubes.

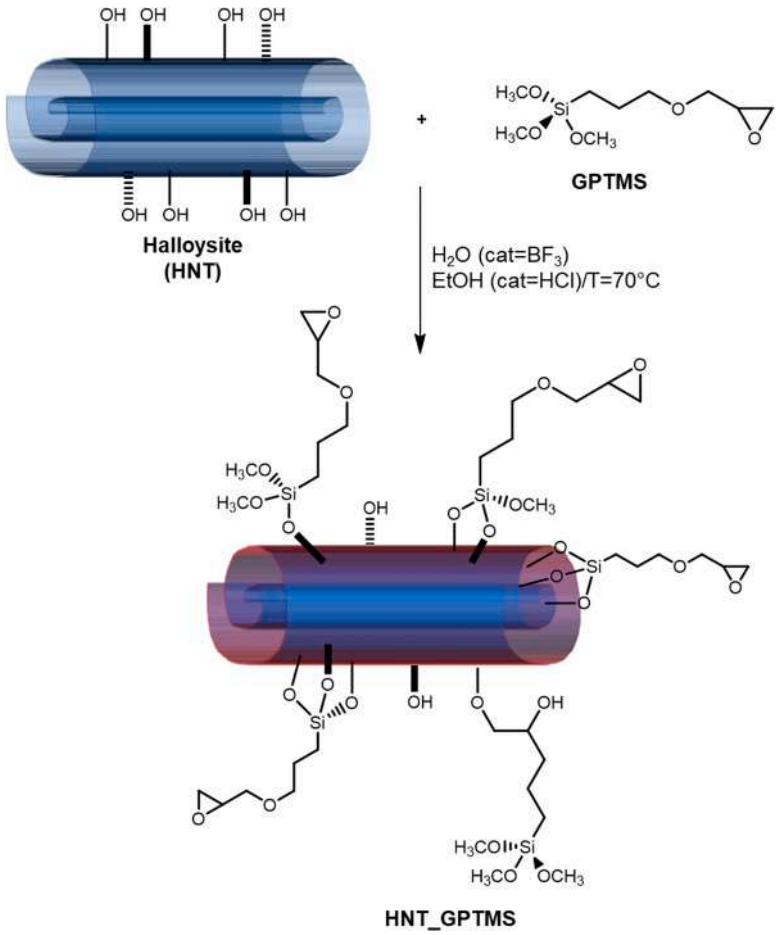

Fig. 2. Reaction scheme for the formation of halloysite derivative functionalized with the GPTMS sols.

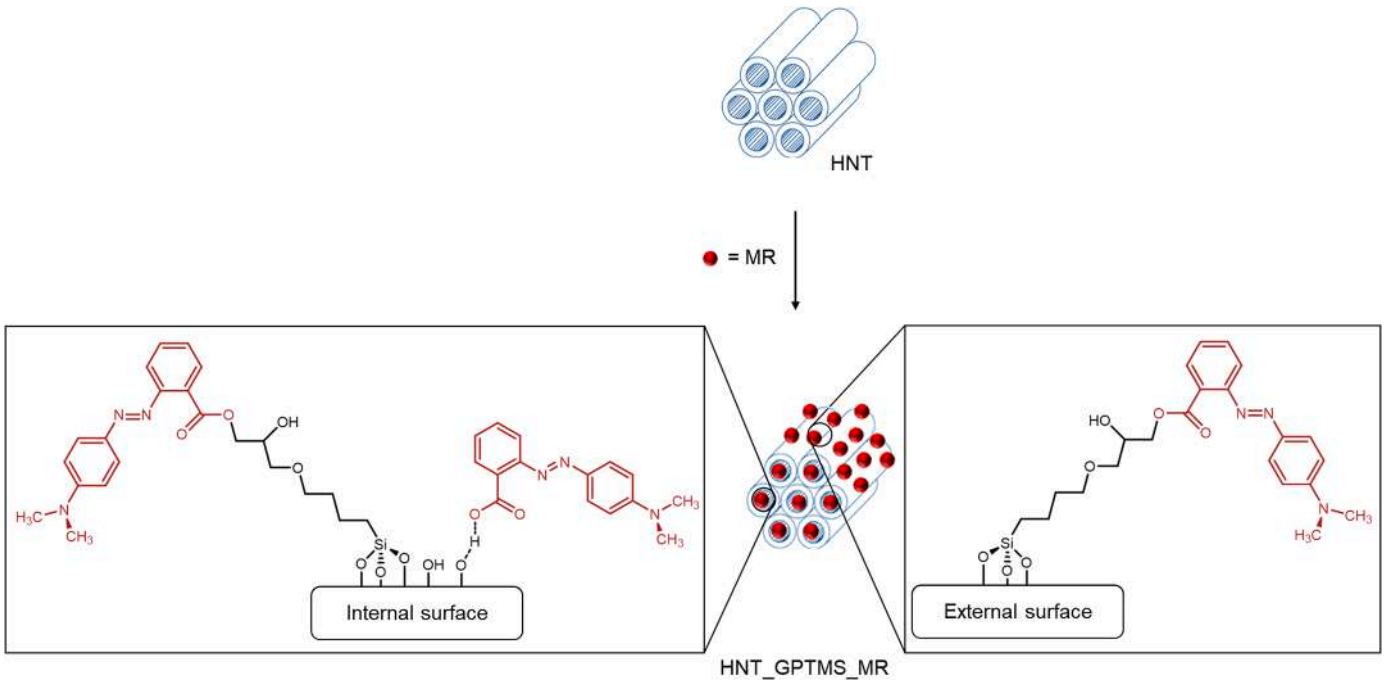

Fig. 3. Schematic representation of the selective functionalization of halloysite by grafting the chromophores on the internal and external surface.

3.2. Functionalized HNTs characterization

3.2.1. NMR characterization of MR-based nanosols

In this work, the attention was focused on the behavior and reactivity of the GPTMS silane precursor in combination with MR dyestuff as a nucleophile. Thus, the obtained adduct was encapsulated into the halloysite nanotubes, used as functional nanofillers to finally stably colour polyester fabrics; these stepwise functionalization reactions were performed in different reaction environments (water or ethanol), to investigate the influence of suitable catalysts ($BF_3O(C_2H_5)$ or HCl, respectively) on the property of the final treated textile samples.

As already shown in other previous work [44], the MR dyestuff reacts as a nucleophile through its carboxylic group towards the GPTMS epoxy ring, giving rise first to an open ring reaction with the formation of the ester adduct GPTMS_MR. Then silane hydrolysis and condensation reactions occur catalyzed by slightly acidic conditions with the formation of the siliceous polymeric network in the presence of HNT (HNT_GPTMS_MR).

In this regard, ^{1}H NMR spectroscopy may be considered a useful tool to monitor the involved reactions and their proceeding in methanol-d_4 solution phase, as well as to characterize the obtained reaction products prior to their application on polyester, i.e. the GPTMS_MR derivative (see Fig. 4) and the nanosol containing the hydrolyzed GPTMS_MR, linked to the HNT filler (HNT_GPTMS_MR), as obtained in situ by reaction of the corresponding starting species in an equimolar ratio (Fig. 5).

The opening of the epoxy ring can be confirmed by observing changes in the signals of the aliphatic protons, particularly the methine H_5 and diastereotopic methylene H_6 protons of the epoxy ring itself (see stacked plot at the top of Fig. 5), which undergo the greatest change in

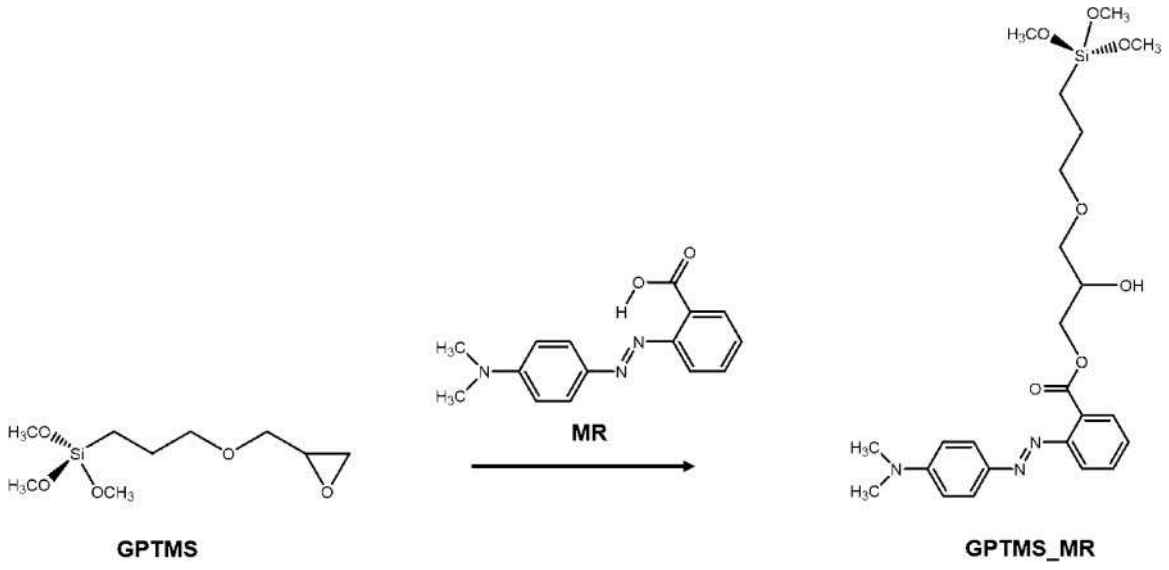

Fig. 4. Reaction scheme related to the formation of the GPTMS_MR ester derivative from GPTMS and MR starting species.

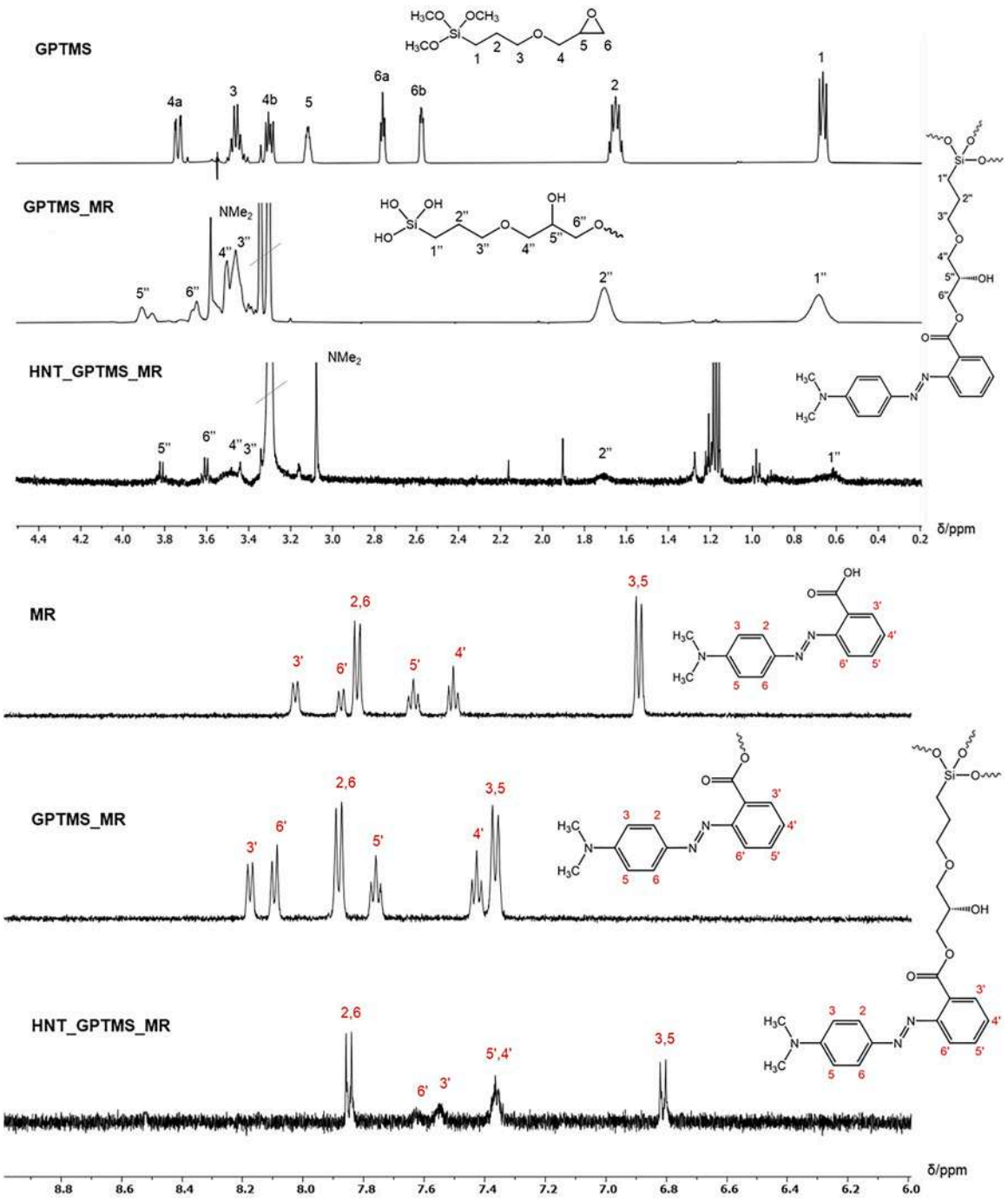

Fig. 5. ^{1}H NMR spectra relative (from top to down) to the aliphatic (upper side) and aromatic region (lower side) of GPTMS and MR signals in starting species and in the two adducts GPTMS_MR and HNT_GPTMS_MR (500 MHz, $T = 298$ K, methanol-d_4).

the two intermediate and final adducts, GPTMS_MR and HNT_GPTMS_MR, respectively. After forming an ester bond with the methyl red dyestuff, both proton chemical shift values (δ/ppm) increase at low fields [44].

In fact, the two diastereotopic methylene protons H_{6a} and H_{6b} go from 2.76 to 2.57 in GPTMS, to 3.65 and 3.60, while the methylene proton H_5 goes from 3.11, to 3.91 and 3.80 in GPTMS_MR and HNT_GPTMS_MR, respectively. Moreover, the simultaneous coalescence of the $H_{6a,b}$ protons in the diol GPTMS derivatives indicates a loosening of the oxirane ring conformational constriction. The hydrolysis reaction brings to the formation of free methanol at 3.55 ppm, and the corresponding Si–O*H* groups, in fast exchange with water (broad peak of water at around 4.5 ppm), which were both saturated by multiple peak suppression in the GPTMS proton spectrum.

In the aromatic zone, all protons move at lower fields, except $H_{4'}$, indicating the establishment of an ester bond with the diol GPTMS derivative. To characterize the adduct HNT_GPTMS_MR, a sample was recorded in the presence of HNT that gives rise to a certain precipitation; all aromatic protons, except $H_{2,6}$, show a different trend moving at lower ppm, i.e. higher field, indicating that they are better shielded.

The different pattern observed for the aromatic protons belonging to GPTMS_MR and HNT_GPTMS_MR may be ascribed to a different orientation of the double bonds of the carboxylic and the diazo groups with the protons of the two benzene rings. In particular, the latter

HNT_GPTMS_MR is most probably immobilized in a plane conformation with the protons benzene ring (i.e. $H_{3'-6'}$) on the same plane of the closest double carboxylic C═O and diazo *N═N* double bonds, being affected by their diamagnetic anisotropic shielding resonance cones, within a preformed polyethyleneoxide (PEO) matrix (whose presence is confirmed by different proton aliphatic patterns [61]).

This experimental finding confirms that in the MR pristine dyestuff, the carboxylic group itself lies in an almost locked six-ring conformation because of the strong hydrogen bond with the nearest nitrogen from the azo bond, as also confirmed by the conformational structure obtained by semi-empirical calculations in an earlier study [44]. Because of this nearly blocked structure, the surrounding resonance cone of both double vicinal bonds has a deshielding effect on the H_3 and $H_{6'}$ aromatic protons of the benzene bearing both *N═N* and C═O functional groups, which consistently causes them to shift downfield toward higher chemical shifts. However, because of the carboxylic group involvement in the ester bond between GPTMS and MR, this hydrogen bond is no longer possible in the GPTMS_MR derivative and even more so in the HNT_GPTMS_MR one. The optimized structure previously described for GPTMS_MR [44] indicates that the two dihedral angles for N–N– $C_{1'}$–$C_{6'}$ and O–C–$C_{2'}$–$C_{3'}$ are somewhat tilted instead of remaining flat. Based on this rationale, the anisotropic resonance cones of the carbonyl and diazo double bonds bring to an observed shielding of their two $H_{3'}$ and $H_{6'}$ ortho benzenic protons, which are now shifted at lower frequencies in the spectra of both GPTMS_MR and HNT_GPTMS_MR.

3.2.2. *FT-IR analysis with total reflectance attenuation of HNT-based nanosols*

To study the chemical structure of the obtained solutions, FT-IR measurements with total reflectance attenuation (ATR) were performed. Halloysite derivatives spectra (Fig. 6) display the characteristic peaks of this nanotubular clay; in particular, the band at 533 cm^{-1} indicates the deformation vibration of Al–O–Si, while the absorption peak at 3438 cm^{-1} is attributed to the O–H stretching of water [62].

The adsorption peak at 911 cm^{-1} can be assigned to the Al–O–OH vibration, while the peaks at 3695 and 3627 cm^{-1} are caused by the stretching vibrations of the inner-surface Al–OH groups [63,64]. A very strong O–Si–O absorption peak was observed at around 1008 cm^{-1}, and the peaks at 674, 747 and 1115 cm^{-1} are assigned to the stretching mode of Si–O [65–68].

The interlayer water can be identified by the bending vibration reflected as the peak at 1608 cm^{-1}. Compared with the FT-IR spectra of HNT raw, the HNT_GPTMS_MR sample clearly shows the functionalization by the selected tri(alkoxy)silane precursor, as evidenced by the presence of C–H_2 asymmetric and symmetric stretching vibrations of alkyl chains present in GPTMS precursor at 2938 and 2869 cm^{-1}.

3.2.3. *Morphological characterization by scanning electron microscopy of HNT-based nanofillers*

To study the morphology of HNT-based nanofillers, SEM analysis was conducted in HV at 5 kV. The EDS (EDAX, Ametek, Tokyo, Japan) investigation was also conducted for the elemental chemical analysis.

Fig. 7 shows the SEM images of the untreated halloysite nanotubes (Fig. 7a) and those treated with GPTMS (Fig. 7b) and GPTMS and Methyl red (Fig. 7c), respectively. EDS spectra are reported in the Figs. 7a–c inserts.

The morphology of HNT was observed to be typical of tubular structures (inset in Fig. 7a).The nanotubes appear stubby, mostly short and thick.

After treatment with GPTMS and with GPTMS and MR, the nanotubes do not appear damaged and retain their nanotubular structure, although the material appears more compact and dense, at the microscopic level. From the EDS analyses, it is possible to observe a higher carbon and silicon peak for the HNT_GPTMS and HNT_GPTMS_MR samples compared to the pristine filler, due to the addition of GPTMS and Methyl red.

3.2.4. *X-ray powder diffraction (XRD) of HNT-based nanofillers*

X-ray diffraction (XRD) is a powerful technique used for the characterization of crystalline materials, including minerals like halloysite. Halloysite is a clay mineral that belongs to the kaolin group, and its crystal structure can be analyzed using XRD.

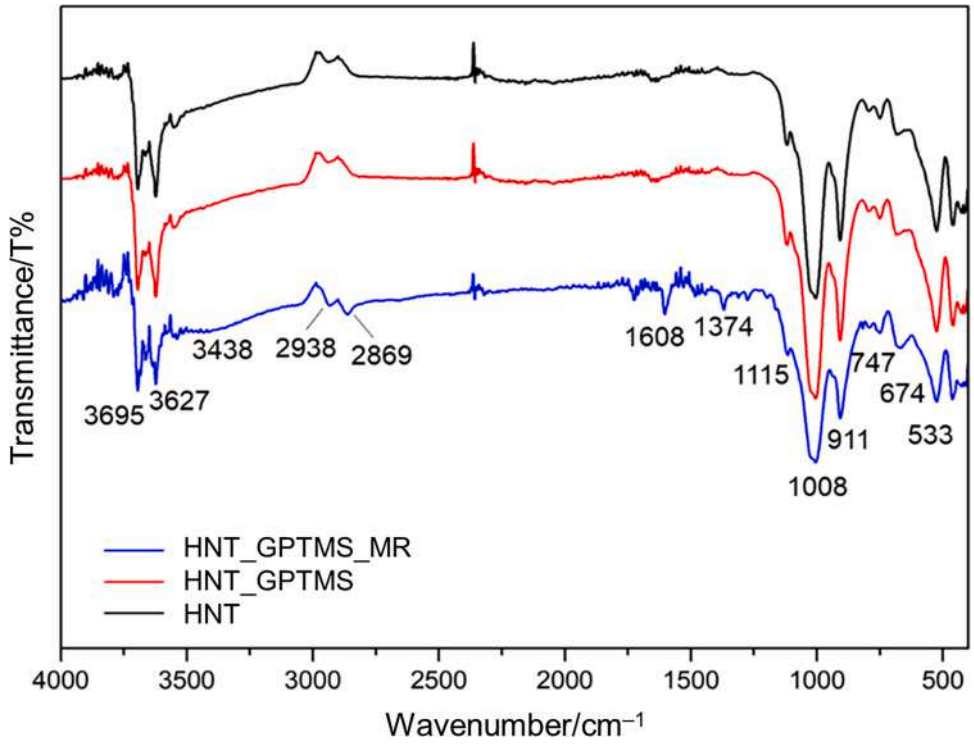

Fig. 6. ATR FT-IR spectra of pristine halloysite clay and their hybrid derivatives after the functionalization with the MR dyestuff and GPTMS precursors.

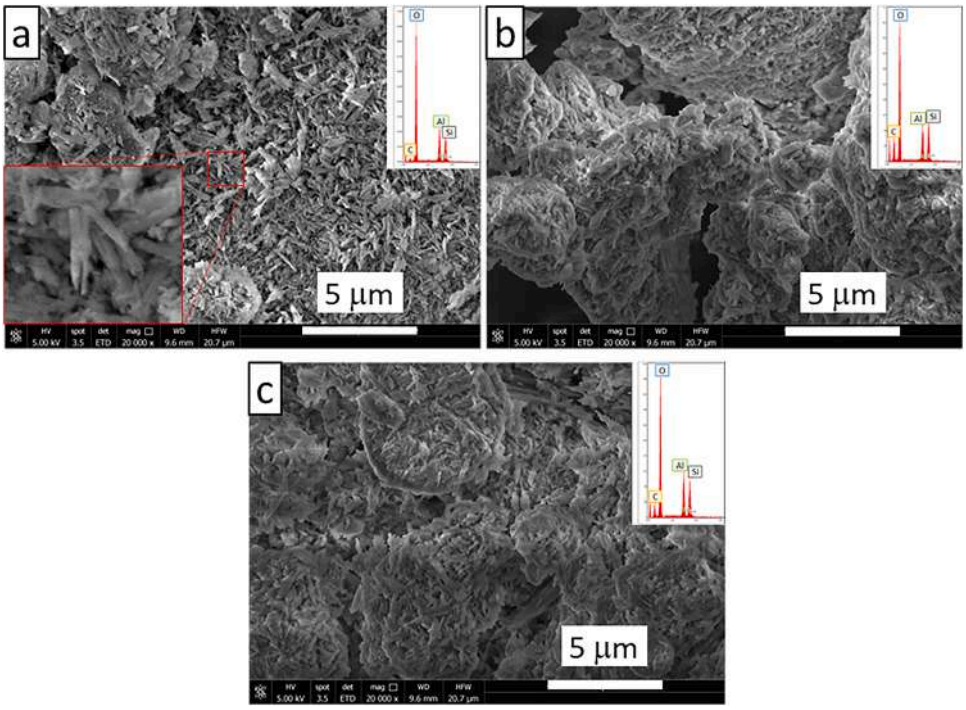

Fig. 7. SEM images of HNT (a), HNT_GPTMS (b) and HNT_GPTMS_MR (c). ESD spectra are represented in the image inserts.

To analyze halloysite nanotubes using XRD, a finely powdered sample is required. The sample should be homogenized to ensure a representative analysis. The powder is then placed on a sample holder, and the surface is levelled for an even distribution.

A typical XRD pattern for halloysite might exhibit the following features:

- The presence of low-angle peaks indicates the presence of a layered structure in halloysite nanotubes. These peaks correspond to the basal reflections and are typically observed at lower 2θ angles.
- One of the characteristic features of halloysite is a peak around 11.8° (2θ), corresponding to the (001) plane of the halloysite crystal lattice.
- Depending on the crystalline form and impurities, you may observe other peaks at higher angles. These peaks are associated with different crystallographic planes and provide information about the crystal structure.

All the characteristic peaks of halloysite are visible in the XRD spectra (Fig. 8). All the samples show similar XRD profiles, indicating that the crystalline structure of HNTs remained almost unchanged after functionalization [69,70], as confirmed by previously described SEM analysis.

For the pure HNT, the XRD pattern displays an intense peak at 11.7 ° with a basal spacing of 0.76 nm for the (001) plane of halloysite, identifying the HNT samples as halloysite-(7 Å). The 2θ positions of 19.8° and 24.8° confirm the dehydrated state, which is characteristic of tubular halloysite with (020) and (002) basal reflection [57].

The characteristic 001 peak of halloysite shifted to a higher 2θ value, compared to pristine HNT, for both HNT_GPTMS (2θ = 11.9°, d-spacing of 0.74 nm) and HNT_GPTMS_MR (2θ = 11.9°, d-spacing of 0.74 nm).

The peak at 19.9° with a basal spacing of 0.45 nm for the (020) plane of halloysite doesn't reveal any particular variation, showing a soft shift to 20.0° with a basal spacing of 0.44 nm for both HNT_GPTMS and HNT_GPTMS_MR samples.

This slight increase in d-spacing is attributed to the functionalization of halloysite by silane molecules [71]. Changes in the (002) plane (2θ = 24.7°) after silylation are also observed with a basal spacing of 0.36 nm, meanwhile for HNT_GPTMS_MR 002 plane corresponds to 24.9 ° with a basal spacing of 0.36 nm. The XRD data provides evidence that the original structure of the HNT was maintained even after surface grafting with the epoxy group of the used organosilane GPTMS.

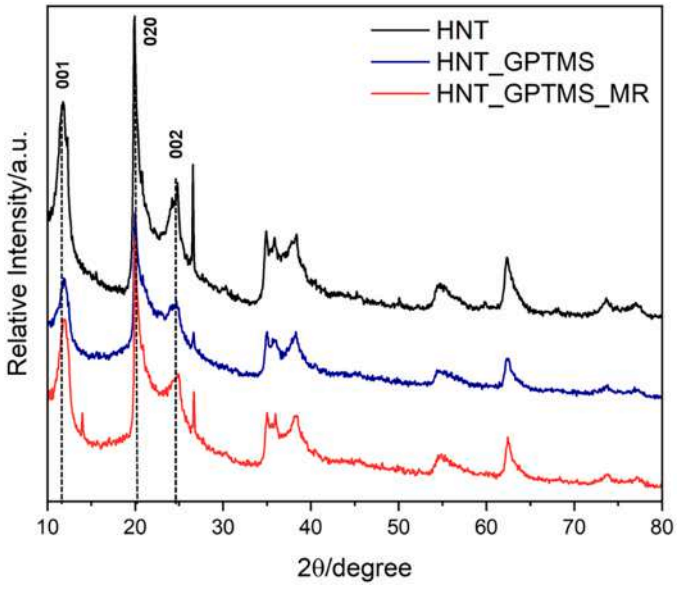

Fig. 8. XRD patterns of pristine HNT (black), HNT_GPTMS (blue) and HNT_GPTMS_MR (red).

3.3. Functionalized fabric analysis

When PE fabrics were treated with HNT_GPTMS_MR, we noticed a different dispersion of the colour (and presumably of the sol) between the coating coming from the aqueous and the ethanolic solution (Fig. 9). As a result, the most homogeneous solution was obtained by applying an

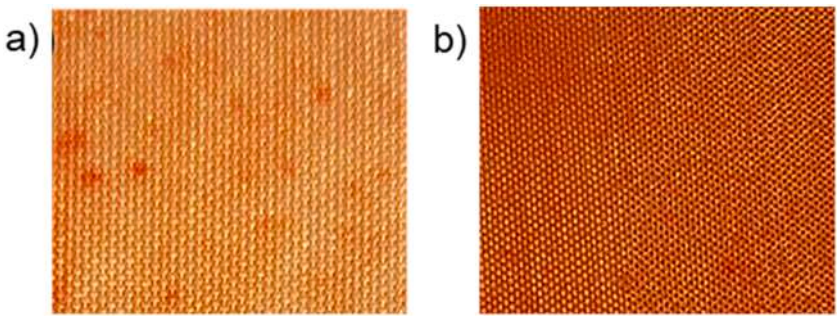

Fig. 9. Dyed polyester samples after deposition of sols containing halloysite nanotubes and GPTMS in aqueous (a) and ethanolic (b) solutions.

ethanolic sol on polyester.

The most interesting aspect is that the use of ethanolic sol containing HNT_GPTMS_MR has allowed, compared to the obtained water sol (see Fig. 9) and to other examples reported so far in the literature, the dyeing of polyester fabrics without using drastic conditions or a pretreatment of textile samples. The evaporation of the solvent and the sol-gel processes, occurring during this time, are clearly evidenced by the colour shift of the fabrics and the colour is resistant to subsequent washing as shown in Fig. 10.

The coloured PE fabrics were characterized by means of different chemical-physical and morphological techniques to ascertain the coating stability.

3.3.1. Morphology analysis by scanning electron microscopy with EDS mapping

The treated and subsequently washed samples were compared to the untreated one, to assess the morphology of the samples after textile finishing and laundry cycles and possible variation in comparison with neat fibres. In Fig. 11, the SEM images of the analyzed samples are reported.

Adding halloysite and GPTMS (Fig. 11b), either in the presence of MR (Fig. 11c), or in the pristine polyester fibres (Fig. 11a), no differences in morphology are noticed. As confirmation of the carried treatment, Si peak is detected in the EDS spectrum of the PE-HNT_GPTMS sample (Fig. 11f). Al element in EDS peaks confirms the presence of halloysite on treated fibres, since aluminum is present only in the structure of clay nanotubes. Even after the tissue washing (Fig. 11d and e, respectively after one and five washes), no damage to fibres is evidenced and the morphology does not change in comparison with Fig. 11c.

Notably, the high homogeneity inferred by the carried treatment, as supported by the EDS mapping (Fig. 12), shows a uniform distribution of Al and Si elements and no phase separation.

3.3.2. AFM morphometry

The nanoscale morphology and qualitative mechanical response of pristine and functionalized PE samples were determined via AFM peak force imaging (Fig. 13). Root mean square surface roughness (S_q) was used as a statistical descriptor of the overall surface morphology, while the root mean square values of the Peakforce inphase signal were used as a semi-quantitative descriptor of local mechanical response, assumed to broadly correspond to surface material inhomogeneity given the nature of these samples.

AFM imaging of pristine PE evidenced marginal local inhomogeneities (resulting in values of $S_q \approx 6$ nm and RMS inphase ≈ 3 mV), which we ascribe to minor wear induced by handling.

All PE-HNT_GPTMS@Et samples have an average S_q comparable to that of pristine PE, but a smaller mechanical inhomogeneity (RMS inphase = 1.0 mV); these values remain largely unaffected even after 5 cycles of washing. This suggests that most material deposited via this functionalization procedure has tightly adhered to the underlying PE fibres.

Before washing, PE-HNT_GPTMS_MR@Et displays a highly homogeneous surface, with both S_q and RMS inphase being one order of magnitude smaller than those of pristine PE. Successive washes induce progressive wear on the surface, first recovering (1 W) and then surpassing (5 W) the degree of local inhomogeneity displayed by pristine PE. This suggests that the amount of material deposited on PE, in this case, was so high as to mask the underlying inhomogeneities but that a consistent proportion of the accreted material was not directly bound to the textile material.

3.3.3. UV–Vis spectral analysis and washing fastness investigation

The diffuse reflectance spectrum of pristine PE samples is reported in Fig. 14 as a black solid curve. In line with the chemical composition of the textile, its spectrum does not present any characteristic feature in the visible region.

This latter observation also holds for PE samples that have been functionalized by treatment with an ethanolic sol of GPTMS-grafted halloysite, their reflectance spectrum (Fig. 14, red line) being entirely superimposable to that of untreated samples. As expected, subjecting the functionalized textiles to one or five washing cycles at 70 °C does not modify the reflective properties of the samples (Fig. 14, bright green and blue lines, respectively) compared to the starting PE. A different picture is obtained when PE samples are treated with an ethanolic sol of GPTMS-

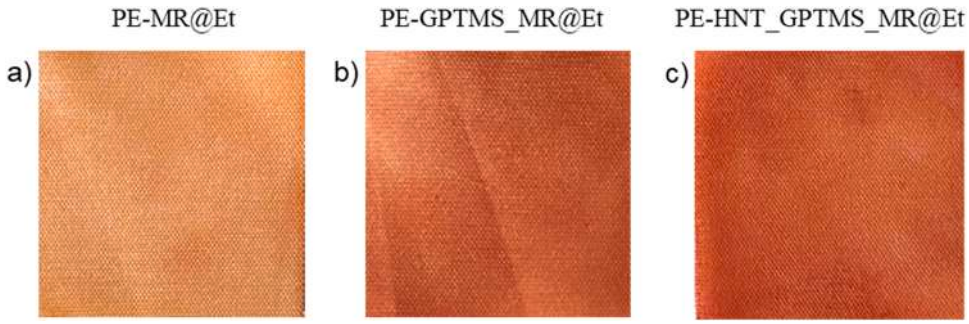

Fig. 10. Coloured polyester after deposition of MR@Et (a), GPTMS_MR@Et (b) and HNT_GPTMS_MR@Et (c) ethanolic solutions.

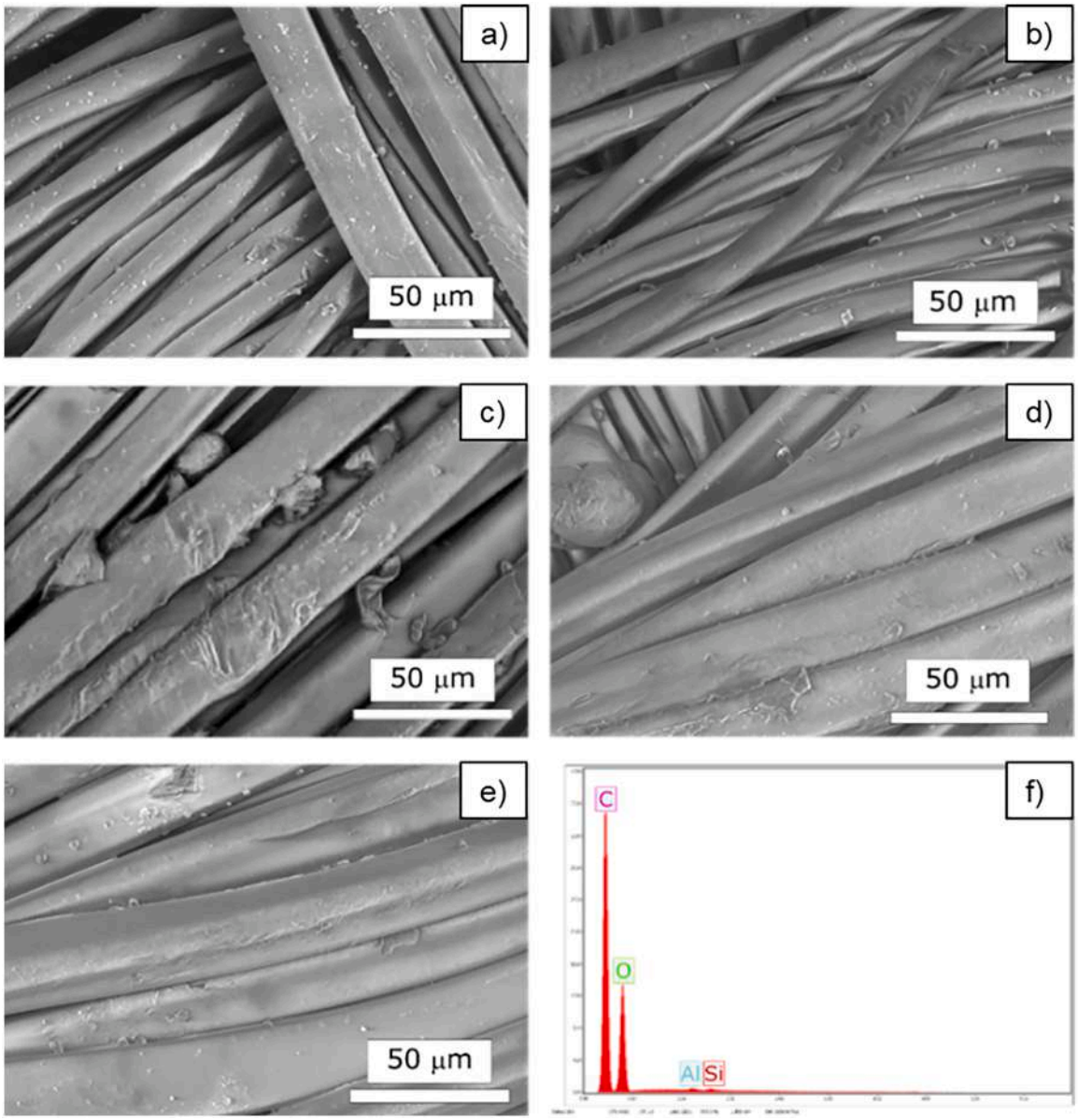

Fig. 11. SEM images of analyzed samples; a) pristine PE, b) PE-HNT_GPTMS@Et, c) PE-HNT_GPTMS_MR@Et, d) PE-HNT_GPTMS_MR@Et_W1, e) PE-HNT_GPTMS_MR@Et_W5, f) EDS of PE-HNT_GPTMS@Et with the corresponding peaks of C, O, Al and Si.

grafted halloysite containing methyl red (Fig. 14, cyan line). Their reflectance spectrum presents a minimum centered at around 470 nm, due to light absorption by the dyestuff, whose absorption spectrum in water (Fig. 14, dashed black line; pH 8) features a maximum in the same spectral region. Just a minimal discolouration, namely a 5 % reduction of the light absorption, is observed upon washing the samples at 70 °C after one washing cycle (Fig. 14, magenta line). In fact, performing additional washing cycles at the same temperature does not further affect the colour of the dyed textiles (Fig. 14, dark green line), indicating that the proposed method is very effective in yielding stable dyestuff loading on PE.

3.3.4. *XPS analysis*

The surface chemical composition of the textile before and after functionalization with HNT_GPTMS@Et was investigated by XPS (Fig. 15).

The survey scan shown in Fig. 15a evidenced that the PE fabric was characterized by the presence of C, O and a small amount of Na, which was considered a contamination of the surface. The C 1 s spectrum (Fig. 15b) is typical of PE, composed of three contributions positioned at BE = 285.0 eV, 286.5 eV and 288.9 eV, and assigned to aliphatic carbon, C–O bond and –COOH(R) group, respectively [72]. While the samples containing HNT_GPTMS@Et and HNT_GPTMS_MR@Et were characterized by the presence of Si from silane (BE = 102.3 eV). It is worth noting that no traces of Al on the surface were detected, indicating that HNT is completely covered with GPTMS.

Moreover, the absorption of MR occurred in the inner layers of the sample, as testified by the absence of the N1s signal due to MR, since XPS is a very surface-sensitive technique (< 10 nm). However, it can be observed that the shape of the C 1 s signal changes when organic compounds were added, increasing the peak intensity in the aliphatic contribution.

3.3.5. *Colour fastness to rubbing and washing*

Colour fastness to washing and rubbing are crucial factors in evaluating the durability of dyed materials, measuring their resistance to washing and friction against a rough surface. In Table 2, the colour coordinates of dyed polyester samples, both unwashed (used as

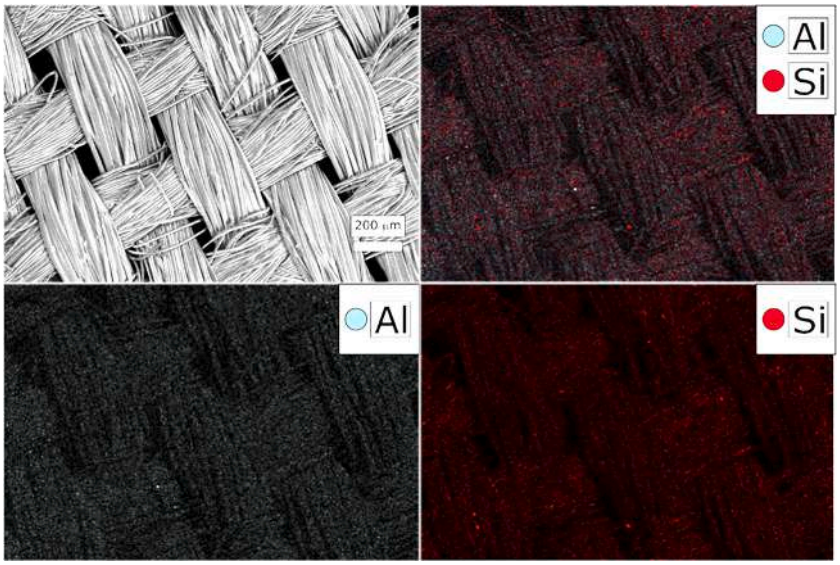

Fig. 12. EDS mapping with the corresponding Al and Si distribution on PE-HNT_GPTMS@Et sample.

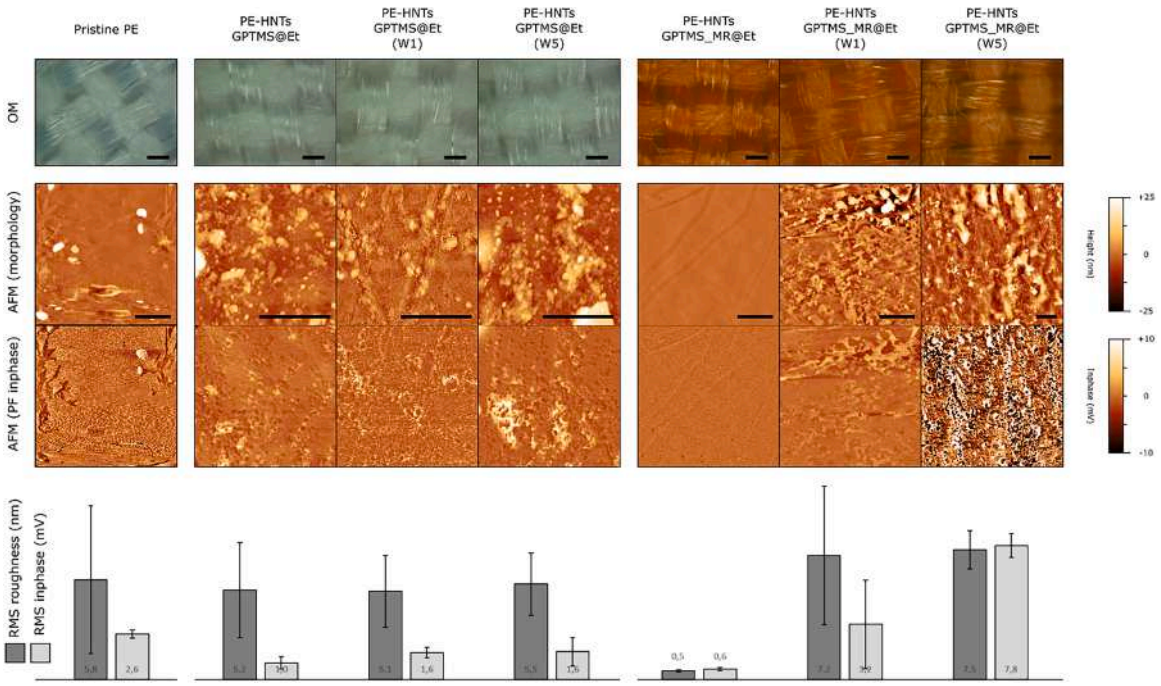

Fig. 13. Nanoscale morphological characterization of pristine and functionalized PE textiles. Top row: representative optical microscopy images; scalebars are 500 µm. Middle row: representative AFM morphology (top) and PeakForce inphase (bottom); scale bars are 1 µm. Bottom row: root mean square roughness S_q (dark grey) and inphase (light grey) as observed via AFM. Error bars are standard deviations from sets of five non-overlapping 1 × 1 µm^2 areas of each sample.

references) and washed, as well as K S^{-1} values and rubbing evaluations according to the greyscale, are reported.

The average colour differences of GPTMS_MR and HNT_GPTMS_MR unwashed polyester fabrics measured at five different positions on the sample indicated very good leveling properties. Moving from unwashed to washed fabrics, there is a noticeable decrease in lightness (L*) values, while the saturation (C*) values remain relatively high, indicating the retention of the dyestuff. In particular, polyester fabrics dyed with GPTMS_MR show a significantly visible colourimetric variation after one wash ($\Delta E^* = 4.53$) due to the leaching of unfixed dye. In contrast, fabrics dyed by GPTMS-grafted halloysite (HNT_GPTMS_MR) show an ΔE^* of 0.95, indicating good colour fastness.

In Table 2, the K S^{-1} equivalent absorption units of unwashed and washed treated fabrics, calculated according to Eq. (3), are presented. The K S^{-1} value represents the intensity of the developed colour; a higher value denotes a deeper developed colour. From the results displayed in Table 2, samples dyed with silane-functionalized MR exhibited a slightly lower colour yield compared to the MR-containing halloysite dyed sample. The colour intensities exhibited by both samples were not statistically different, suggesting similar colourability. Dye levelness was assessed using Eq. (4), where a lower $S\gamma(\lambda)$ value indicates a higher level dyeing property. The experiment demonstrated that the values obtained by the halloysite-assisted dyeing process were lower than those obtained by dyeing polyester samples with silane-functionalized MR, regardless of washing cycles (Fig. 16 and Table 2).

Results showed that GPTMS_MR-dyed polyester, with an initial K S^{-1}

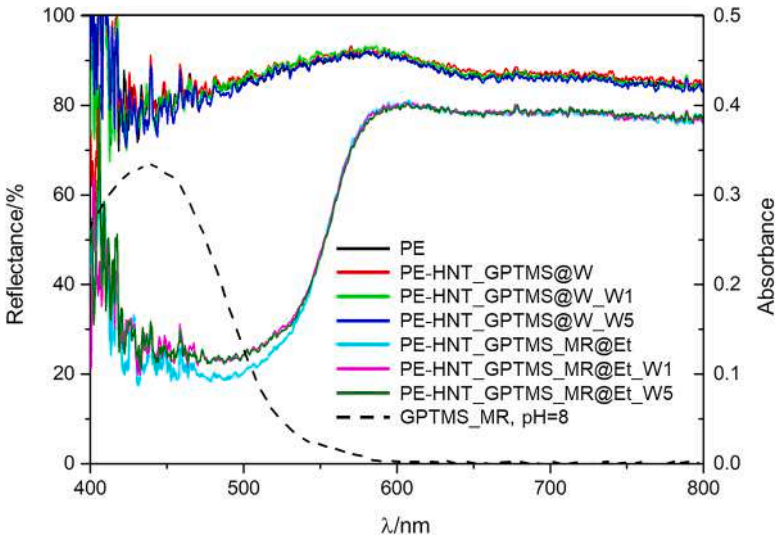

Fig. 14. Diffuse reflectance of PE samples functionalized with (i) an ethanolic sol of GPTMS-grafted halloysite (red, bright green and blue lines) or (ii) an ethanolic sol of GPTMS-grafted halloysite containing methyl red (cyan, magenta and dark green lines). The spectra have been recorded before (red and cyan lines) and after one (light green and magenta lines) or five (blue and dark green lines) washing cycles at 70 °C. The reflectance spectrum of pristine PE (solid black line) and the absorption spectrum of a water solution of methyl red at pH 8 (dashed black line, right y-axis) have been included as a reference.

of 3.23 and a maximum variation of $S\gamma(\lambda)$ value of +0.07, was reduced to 2.41 with a $S\gamma(\lambda)$ value of +0.08 after one washing cycle, indicating a 25.4 % loss in fastness. After five laundering cycles, the fastness rate increased to 31.6 %, resulting in a $S\gamma(\lambda)$ value of +0.09. Conversely, the MR-containing halloysite dyed samples exhibited a better fastness percentage, as the initial colour strength decreased from 4.05 to 3.55 after one wash (a 12.3 % loss in fastness). Moreover, the dye leaching was slightly reduced when fabrics were treated with the HNT-encapsulated GPTMS_MR, resulting in an 11.1% loss in colour fastness after five washes. The $S\gamma(\lambda)$ value of the unwashed halloysite-containing sample was +0.05, maintained at +0.06 after one and five washing cycles. Therefore, with the assistance of the halloysite, there was little enhancement in the colour depth of the dyed fabric and a slight improvement in dyeing uniformity.

However, results from the dyed samples indicated that there is no significant difference in colour strength due to the encapsulation of MR in halloysite molecules, which is also visible to the naked eye (Fig. 17). This finding suggests that the presence of halloysite does not limit the diffusion of dyes into the polyester fibres compared to the dyeing procedure using GPTMS_MR. Moreover, data reported in Table 2 highlight the improved durability of the GPTMS-functionalized MR coatings on polyester fabrics when in the presence of the selected nanofiller thanks to its higher ability to anchor the dye.

As shown in Fig. 17, all dyed polyester fabrics exhibit good dry crocking fastness. Notably, the results under wet conditions are particularly significant. Generally, when the white crocking cotton samples are wetted their fibres swell leading to increased friction and a large contact area, which can result in more mechanical action during the wet crocking operation. Consequently, in wet crocking conditions dye particles are often more easily removed by the wet white crocking cloth. However, during the crocking tests under wet conditions, no ablation phenomena were observed. The wetted white crocking cotton samples did not show any traces of colouration, and a consistent crocking rating was assigned for all samples.

4. Conclusions

In this paper, a "bottom-up" process was used to develop MR-loaded halloysite nanotubes functionalized by GPTMS as an innovative dyeing strategy of polyester fabrics. As a matter of fact, PE samples were dyed with the so-obtained halloysite-containing silica hybrid film by means of impregnation-thermofixation padding-based method, which is currently used in many textile finishing processes to treat synthetic fibres.

In particular, the study of the reaction between the alkoxysilane, the nano-sized HNT filler and the fabric has proven to be of key importance in the immobilization of the methyl red, loaded in halloysite nanotubes and chemically encapsulated in a hybrid silane matrix, which results in a dense microstructure which reduces the dyestuff leaching. NMR experiments revealed the structure of the organic-inorganic hybrid molecule resulting from the sol-gel reaction in ethanol, confirming the success of the dyestuff coordination reaction to the 3D matrix.

Moreover, the MR-silica based coatings developed by padding-cure method provide good contact with the fibres and adhesion of the hybrid film to the surface of the textile fabrics. The SEM analysis showed the effects of the treatment on the morphology of the fabric fibres, highlighting how the treatment with GPTMS-based sol modified the microstructure of the fibres and how the dispersion of the sol was homogeneous. The dyeing method developed in this study offers many advantages over traditional aqueous dyeing: high-quality dyed goods without the need for auxiliaries and large amounts of water, as well as the potential reduction of both surface oligomers and micro- or nanofibre release during maintenance cycles, being also satisfactory in terms of fastness properties of the dyed modified PE fabrics. Finally, fastness to washing and rubbing, in the latter case both under dry and wet conditions, exhibited excellent values, achieving a rating of 5 for all investigated samples according to the geometric grey scale. Overall, the experimental findings suggest that the halloysite-based dyeing technique is a promising alternative to conventional processes for the uniform colouration of polyester fabrics. Therefore this study could open the way to a new approach to dyeing polyester fabrics with acid dyes through halloysite-assisted anchoring hosts, at reduced temperatures and shorter durations, as opposed to conventional dyeing methods of polyester fibres.

Funding sources

This work has been partially funded by European Union (NextGeneration EU), through the MUR-PNRR project SAMOTHRACE (SiciliAn MicronanOTecH Research And Innovation Center, ECS00000022) and the MICS (Made in Italy–Circular and Sustainable) Extended Partnership and received funding from the European Union Next-Generation EU (PIANO NAZIONALE DI RIPRESA E RESILIENZA (PNRR) –MISSIONE 4

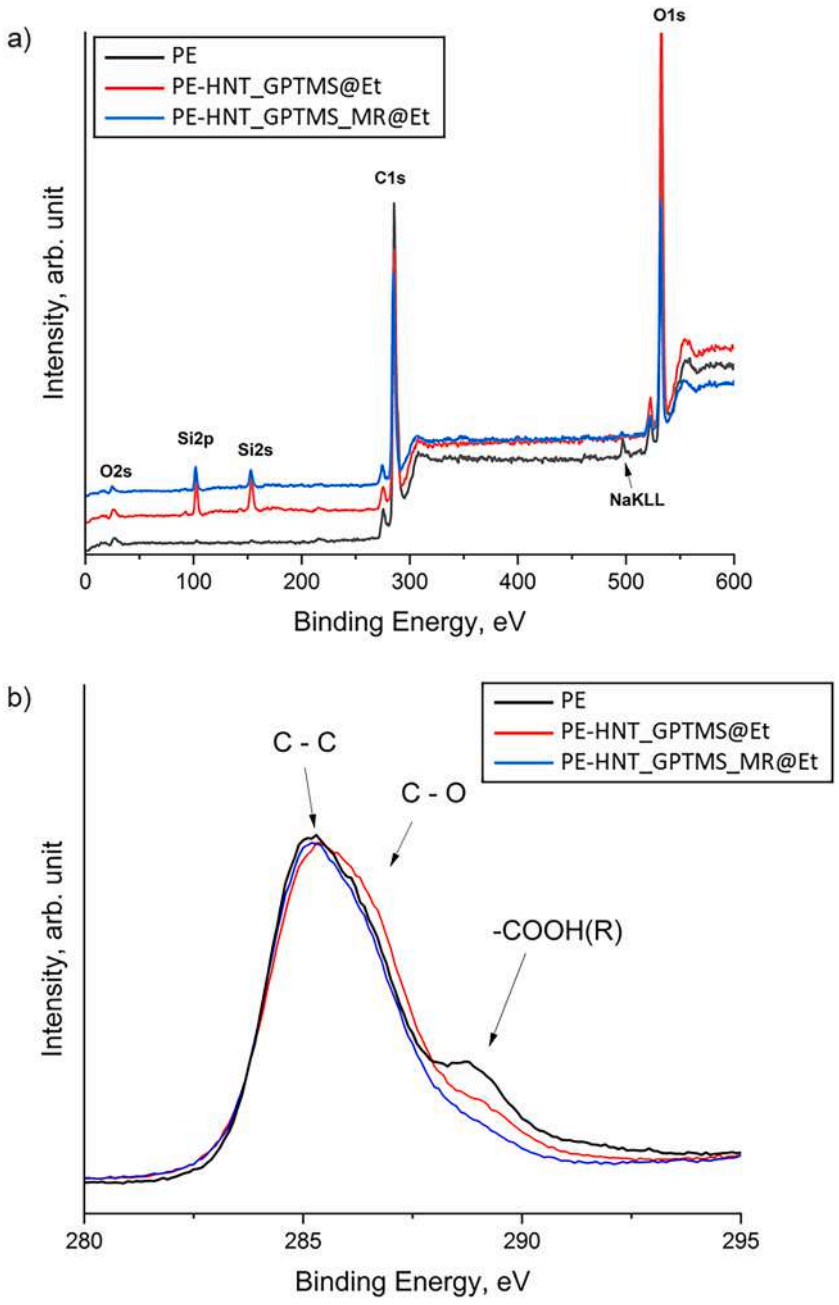

Fig. 15. XPS spectra comparison of (a) surveys and (b) C 1 s of the textile before and after treatment.

Table 2
Washing and rubbing fastness properties of dyed polyester fabrics. ΔE* was calculated according to eq. (2), comparing the washed sample (after 1 or 5 laundering cycles) to the original unwashed dyed fabric (reference).

Textile samples	Wash fastness					K S^{-1}	Sγ(λ)	Rubbing fastness	
	L*	a*	b*	ΔE*	C*			dry	wet
PE-GPTMS_MR@Et	70.38	50.07	48.88	–	69.98	3.23	0.07	5	5
PE-GPTMS_MR@Et_W1	69.67	47.80	45.02	4.53	65.66	2.41	0.08	5	5
PE- GPTMS_MR@Et_W5	68.45	48.50	46.42	3.50	67.13	2.21	0.09	5	5
PE-HNT_GPTMS_MR@Et	70.36	50.05	48.15	–	70.69	4.05	0.05	5	5
PE-HNT_GPTMS_MR@Et_W1	70.01	49.23	47.81	0.95	69.50	3.55	0.06	5	5
PE-HNT_GPTMS_MR@Et_W5	69.75	48.59	47.01	1.95	63.19	3.60	0.06	5	5

COMPONENTE 2, INVESTIMENTO 1.3 –D.D. 1551.11–10–2022, PE00000004). This manuscript reflects only the authors' views and opinions, neither the European Union nor the European Commission can be considered responsible for them.

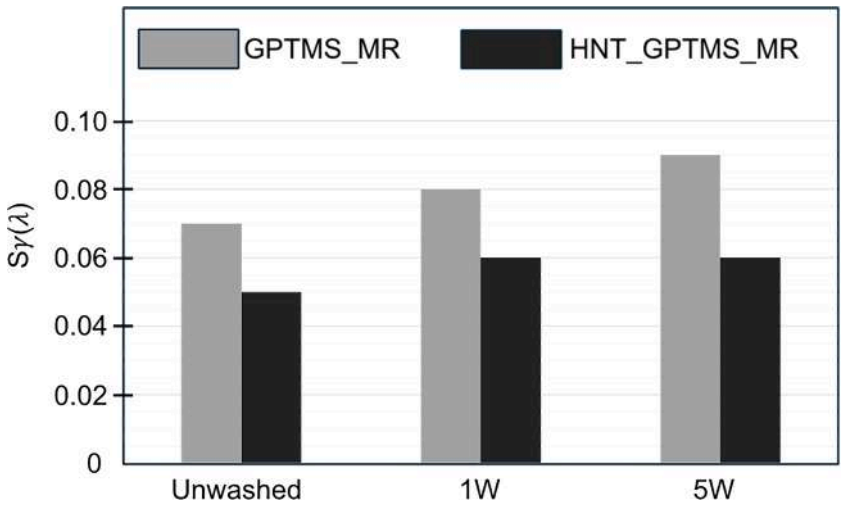

Fig. 16. Level dyeing property of GPTMS_MR and HNT_GPTMS_MR dyed polyester fabrics (Sγ(λ)).

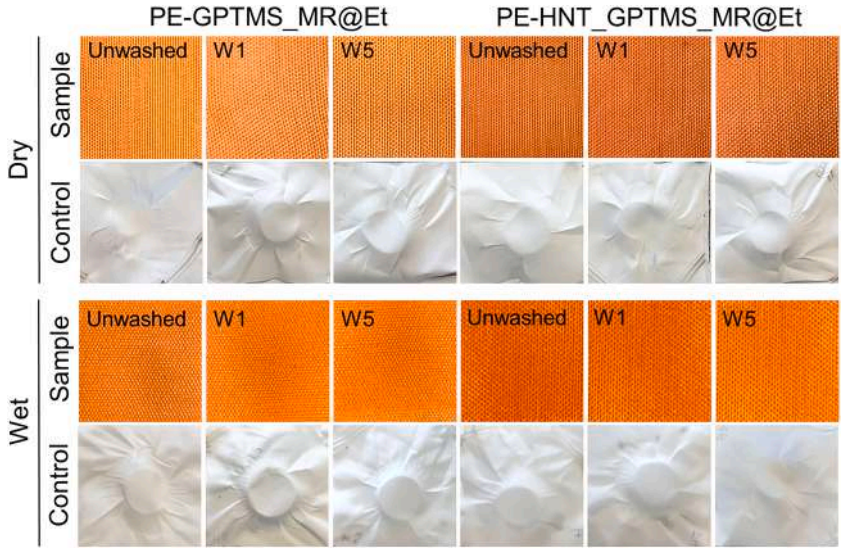

Fig. 17. Images of polyester fabrics dyed with GPTMS_MR and HNT_GPTMS_MR after rubbing fastness test, both in dry and wet conditions, and corresponding control fabrics. After testing in wet conditions, sample images appear darkened due to contact with the wet control fabric.

Author agreement statement

I hereby certify that Giulia Rando, Silvia Sfameni, Mariam Hadhri, Alessio Mezzi, Marco Brucale, Giovanna De Luca, Elpida Piperopolus, Candida Milone, Dario Drommi, Giuseppe Rosace, Valentina Trovato and I are the sole authors of this manuscript, and that manuscript is original, has not been published before and is not currently being considered for publication elsewhere.

I confirm that the manuscript has been read and approved by all named authors and that there are no other persons who satisfied the criteria for authorship but are not listed. I further confirm that the order of authors listed in the manuscript has been approved by all of us. I understand that the Corresponding Author is the sole contact for the Editorial process, and that I am responsible for communicating with the other authors about progress, submissions of revisions and final approval of proofs. I certify that, to the best of my knowledge, this manuscript does not infringe upon anyone's copyright nor violate any proprietary rights and that any ideas, techniques, quotations, or any other material from the work of other people included in this manuscript, published or otherwise, are fully acknowledged in accordance with the standard referencing practices.

No generative AI and AI-assisted technologies was used in the writing process.

CRediT authorship contribution statement

Giulia Rando: Writing – review & editing, Writing – original draft, Data curation, Conceptualization. **Silvia Sfameni:** Writing – review & editing, Writing – original draft, Data curation, Conceptualization. **Mariam Hadhri:** Writing – review & editing, Writing – original draft, Data curation, Conceptualization. **Alessio Mezzi:** Writing – review & editing, Writing – original draft, Data curation. **Marco Brucale:** Writing – review & editing, Writing – original draft, Data curation. **Giovanna De Luca:** Writing – review & editing, Writing – original draft, Data curation. **Elpida Piperopoulos:** Writing – review & editing, Writing – original draft, Data curation. **Candida Milone:** Writing – review & editing, Writing – original draft, Data curation. **Dario Drommi:** Writing – original draft, Data curation. **Giuseppe Rosace:** Writing – review & editing, Writing – original draft, Supervision, Resources, Data curation, Conceptualization. **Valentina Trovato:** Writing – review & editing, Writing – original draft, Data curation, Conceptualization. **Maria Rosaria Plutino:** Writing – review & editing, Writing – original draft,

Supervision, Resources, Data curation, Conceptualization.

Declaration of competing interest

The authors declare that they have no known competing financial interests or personal relationships that could have appeared to influence the work reported in this paper.

Data availability

Data will be made available on request.

Acknowledgment

MURST: CNR and MUR, and FOE 2022—Future Raw Materials are gratefully acknowledged. All authors wish to thank S. Romeo, G. Napoli, G. Bellanti and F. Giordano for technical and informatic assistance in all instrumentation set-up and subsequent data fitting.

References

[1] V. Trovato, S. Sfameni, R. Ben Debabis, G. Rando, G. Rosace, G. Malucelli, M. R. Plutino, How to address flame-retardant technology on cotton fabrics by using functional inorganic sol-gel precursors and nanofillers: flammability insights, research advances, and sustainability challenges, Inorganics 11 (2023), https://doi.org/10.3390/inorganics11070306.
[2] G. Rando, S. Sfameni, M.R. Plutino, Development of functional hybrid polymers and gel materials for sustainable membrane-based water treatment technology: how to combine greener and cleaner approaches, Gels 9 (2023), https://doi.org/10.3390/gels9010009.
[3] W.O. Yah, A. Takahara, Y.M. Lvov, Selective modification of halloysite lumen with octadecylphosphonic acid: new inorganic tubular micelle, J. Am. Chem. Soc. 134 (2012) 1853–1859, https://doi.org/10.1021/ja210258y.
[4] R. Zhai, B. Zhang, L. Liu, Y. Xie, H. Zhang, J. Liu, Immobilization of enzyme biocatalyst on natural halloysite nanotubes, Catal. Commun. 12 (2010) 259–263, https://doi.org/10.1016/j.catcom.2010.09.030.
[5] U.A. Handge, K. Hedicke-Höchstötter, V. Altstädt, Composites of polyamide 6 and silicate nanotubes of the mineral halloysite: influence of molecular weight on thermal, mechanical and rheological properties, Polymer (Guildf) 51 (2010) 2690–2699, https://doi.org/10.1016/j.polymer.2010.04.041.
[6] H. Chen, J. Zhao, J. Wu, H. Yan, Selective desorption characteristics of halloysite nanotubes for anionic azo dyes, RSC Adv 4 (2014) 15389–15393, https://doi.org/10.1039/C3RA47561A.
[7] G. Rando, S. Sfameni, M. Galletta, D. Drommi, S. Cappello, M.R. Plutino, Functional nanohybrids and nanocomposites development for the removal of environmental pollutants and bioremediation, Mol (2022) 27, https://doi.org/10.3390/molecules27154856.
[8] P. Luo, Y. Zhao, B. Zhang, J. Liu, Y. Yang, J. Liu, Study on the adsorption of Neutral Red from aqueous solution onto halloysite nanotubes, Water Res 44 (2010) 1489–1497, https://doi.org/10.1016/j.watres.2009.10.042.
[9] F. Liu, L. Bai, H. Zhang, H. Song, L. Hu, Y. Wu, X. Ba, Smart H2O2-responsive drug delivery system made by halloysite nanotubes and carbohydrate polymers, ACS Appl. Mater. Interfaces 9 (2017) 31626–31633, https://doi.org/10.1021/acsami.7b10867.
[10] Y. Joo, J.H. Sim, Y. Jeon, S.U. Lee, D. Sohn, Opening and blocking the inner-pores of halloysite, Chem. Commun. 49 (2013) 4519–4521, https://doi.org/10.1039/C3CC40465J.
[11] L. Yu, H. Wang, Y. Zhang, B. Zhang, J. Liu, Recent advances in halloysite nanotube derived composites for water treatment, Environ. Sci. Nano 3 (2016) 28–44, https://doi.org/10.1039/C5EN00149H.
[12] V. Trovato, S. Sfameni, G. Rando, G. Rosace, S. Libertino, A. Ferri, M.R. Plutino, A review of stimuli-responsive smart materials for wearable technology in healthcare: retrospective, perspective, and prospective, Molecules (2022) 27, https://doi.org/10.3390/molecules27175709.
[13] F. Giacobello, I. Ielo, H. Belhamdi, M.R. Plutino, Geopolymers and functionalization strategies for the development of sustainable materials in construction industry and cultural heritage applications: a review, Materials (Basel) 15 (2022), https://doi.org/10.3390/ma15051725.
[14] G.S. Machado, K.A.D. de Freitas Castro, F. Wypych, S. Nakagaki, Immobilization of metalloporphyrins into nanotubes of natural halloysite toward selective catalysts for oxidation reactions, J. Mol. Catal. A Chem. 283 (2008) 99–107, https://doi.org/10.1016/j.molcata.2007.12.009.
[15] E. Joussein, S. Petit, B. Delvaux, Behavior of halloysite clay under formamide treatment, Appl. Clay Sci. 35 (2007) 17–24, https://doi.org/10.1016/j.clay.2006.07.002.
[16] G. Cavallaro, L. Chiappisi, P. Pasbakhsh, M. Gradzielski, G. Lazzara, A structural comparison of halloysite nanotubes of different origin by Small-Angle Neutron Scattering (SANS) and Electric Birefringence, Appl. Clay Sci. 160 (2018) 71–80.
[17] J. Huang, Z.H. Tang, X.H. Zhang, B.C. Guo, Halloysite polymer nanocomposites. Dev. Clay Sci, Elsevier, 2016, pp. 509–553.
[18] M. Massaro, S. Riela, G. Cavallaro, M. Gruttadauria, S. Milioto, R. Noto, G. Lazzara, Eco-friendly functionalization of natural halloysite clay nanotube with ionic liquids by microwave irradiation for Suzuki coupling reaction, J. Organomet. Chem. 749 (2014) 410–415.
[19] G. Lazzara, G. Cavallaro, A. Panchal, R. Fakhrullin, A. Stavitskaya, V. Vinokurov, Y. Lvov, An assembly of organic-inorganic composites using halloysite clay nanotubes, Curr. Opin. Colloid Interface Sci. 35 (2018) 42–50, https://doi.org/10.1016/j.cocis.2018.01.002.
[20] V. Bertolino, G. Cavallaro, S. Milioto, G. Lazzara, Polysaccharides/Halloysite nanotubes for smart bionanocomposite materials, Carbohydr. Polym. 245 (2020) 116502, https://doi.org/10.1016/j.carbpol.2020.116502.
[21] C. Zhang, D.A. Mcadams 2nd, J.C. Grunlan, Nano/Micro-Manufacturing of Bioinspired Materials: a Review of Methods to Mimic Natural Structures, Adv. Mater. 28 (2016) 6292–6321, https://doi.org/10.1002/adma.201505555.
[22] D.A. Prishchenko, E.V. Zenkov, V.V. Mazurenko, R.F. Fakhrullin, Y.M. Lvov, V. G. Mazurenko, Molecular dynamics of the halloysite nanotubes, Phys. Chem. Chem. Phys. 20 (2018) 5841–5849.
[23] A.C. Santos, C. Ferreira, F. Veiga, A.J. Ribeiro, A. Panchal, Y. Lvov, A. Agarwal, Halloysite clay nanotubes for life sciences applications: from drug encapsulation to bioscaffold, Adv. Colloid Interface Sci. 257 (2018) 58–70.
[24] M. Massaro, G. Lazzara, R. Noto, S. Riela, Halloysite nanotubes: a green resource for materials and life sciences, Rend. Lincei. Sci. Fis. e Nat. 31 (2020) 213–221, https://doi.org/10.1007/s12210-020-00886-x.
[25] M. Massaro, F. Armetta, G. Cavallaro, D.F. Chillura Martino, M. Gruttadauria, G. Lazzara, S. Riela, M. d'Ischia, Effect of halloysite nanotubes filler on polydopamine properties, J. Colloid Interface Sci. 555 (2019) 394–402, https://doi.org/10.1016/j.jcis.2019.07.100.
[26] S. Sfameni, G. Rando, M.R. Plutino, Sustainable secondary-raw materials, natural substances and eco-friendly nanomaterial-based approaches for improved surface performances: an overview of what they are and how they work, Int. J. Mol. Sci. (2023) 24, https://doi.org/10.3390/ijms24065472.
[27] T.A. Otitoju, A.L. Ahmad, B.S. Ooi, Recent advances in hydrophilic modification and performance of polyethersulfone (PES) membrane via additive blending, RSC Adv 8 (2018) 22710–22728, https://doi.org/10.1039/C8RA03296C.
[28] G. Cavallaro, G. Lazzara, S. Milioto, Dispersions of nanoclays of different shapes into aqueous and solid biopolymeric matrices, Extended Physicochemical Study, Langmuir 27 (2011) 1158–1167, https://doi.org/10.1021/la103487a.
[29] P. Yuan, P.D. Southon, Z. Liu, M.E.R. Green, J.M. Hook, S.J. Antill, C.J. Kepert, Functionalization of halloysite clay nanotubes by grafting with γ-aminopropyltriethoxysilane, J. Phys. Chem. C 112 (2008) 15742–15751.
[30] D. Tan, P. Yuan, D. Liu, P. Du, Chapter 8 - Surface Modifications of Halloysite, in: P. Yuan, A. Thill, F.B.T. -D, C.S. Bergaya (Eds.), Nanosized Tubul. Clay Miner, Elsevier, 2016, pp. 167–201, https://doi.org/10.1016/B978-0-08-100293-3.00008-X.
[31] A.F. Peixoto, A.C. Fernandes, C. Pereira, J. Pires, C. Freire, Physicochemical characterization of organosilylated halloysite clay nanotubes, Microporous Mesoporous Mater 219 (2016) 145–154, https://doi.org/10.1016/j.micromeso.2015.08.002.
[32] S. Sfameni, M. Hadhri, G. Rando, D. Drommi, G. Rosace, V. Trovato, M.R. Plutino, Inorganic Finishing for Textile Fabrics: recent Advances in Wear-Resistant, UV Protection and Antimicrobial Treatments, Inorganics 11 (2023), https://doi.org/10.3390/inorganics11010019.
[33] N. Lama, J. Wilhite, Y. Lvov, S. Konnova, R. Fakhrullin, Clay nanotube coating on cotton fibers for enhanced flame-retardancy and antibacterial properties, ChemNanoMat 9 (2023) e202300106, https://doi.org/10.1002/cnma.202300106.
[34] Y. Feng, Y. He, X. Lin, M. Xie, M. Liu, Y. Lvov, Assembly of clay nanotubes on cotton fibers mediated by biopolymer for robust and high-performance hemostatic dressing, Adv. Healthc. Mater. 12 (2023) 2202265, https://doi.org/10.1002/adhm.202202265.
[35] R.M. Frazier, K.A. Vivas, I. Azuaje, R. Vera, A. Pifano, N. Forfora, H. Jameel, E. Ford, J.J. Pawlak, R. Venditti, R. Gonzalez, Beyond cotton and polyester: an Evaluation of emerging feedstocks and conversion methods for the future of fashion industry, J. Bioresour. Bioprod. (2024), https://doi.org/10.1016/j.jobab.2024.01.001.
[36] T. Salem, F. Simon, A.A. El-Sayed, M. Salama, Plasma-assisted surface modification of polyester fabric for developing halochromic properties, Fibers Polym. 18 (2017) 731–740. https://doi.org/10.1007/s12221-017-6858-8.
[37] K. El-Nagar, M.A. Saudy, A.I. Eatah, M.M. Masoud, DC pseudo plasma discharge treatment of polyester textile surface for disperse dyeing, J. Text. Inst. 97 (2006) 111–117, https://doi.org/10.1533/joti.2005.0169.
[38] V. Trovato, A. Mezzi, M. Brucale, H. Abdeh, D. Drommi, G. Rosace, M.R. Plutino, Sol-gel assisted immobilization of alizarin red s on polyester fabrics for developing stimuli-responsive wearable sensors, Polymers (Basel) 14 (2022), https://doi.org/10.3390/polym14142788.
[39] J.R. Aspland, Disperse dyes and their application to polyester, Text. Chem. Color. 24 (1992) 18.
[40] R. Shamey, W.S. Shim, Assessment of key issues in the coloration of polyester material, Text. Prog. 43 (2011) 97–153, https://doi.org/10.1080/00405167.2011.565151.
[41] İ. Şener, N. Şener, M. Gür, Synthesis, structural analysis, and absorption properties of disperse benzothiazol-derivative mono-azo dyes, J. Mol. Struct. 1174 (2018) 12–17, https://doi.org/10.1016/j.molstruc.2018.04.052.
[42] M.R. Maliyappa, J. Keshavayya, M. Mahanthappa, Y. Shivaraj, K.V. Basavarajappa, 6-Substituted benzothiazole based dispersed azo dyes having pyrazole moiety:

synthesis, characterization, electrochemical and DFT studies, J. Mol. Struct. 1199 (2020) 126959, https://doi.org/10.1016/j.molstruc.2019.126959.
[43] P.T. Tasli, Ç.K. Atay, T. Demirturk, T. Tilki, Experimental and computational studies of newly synthesized azo dyes based materials, J. Mol. Struct. 1201 (2020) 127098, https://doi.org/10.1016/j.molstruc.2019.127098.
[44] M.R. Plutino, E. Guido, C. Colleoni, G. Rosace, Effect of GPTMS functionalization on the improvement of the pH-sensitive methyl red photostability, Sensors Actuators B 238 (2017) 281–291, https://doi.org/10.1016/j.snb.2016.07.050.
[45] S. Sfameni, T. Lawnick, G. Rando, A. Visco, T. Textor, M.R. Plutino, Super-Hydrophobicity of Polyester Fabrics Driven by Functional Sustainable Fluorine-Free Silane-Based Coatings, Gels 9 (2023), https://doi.org/10.3390/gels9020109.
[46] S. Sfameni, A. Del Tedesco, G. Rando, F. Truant, A. Visco, M.R. Plutino, Waterborne Eco-Sustainable Sol-Gel Coatings Based on Phytic Acid Intercalated Graphene Oxide for Corrosion Protection of Metallic Surfaces, Int. J. Mol. Sci. 23 (2022), https://doi.org/10.3390/ijms231912021.
[47] A. Khatri, M. White, 5 - Sustainable dyeing technologies, in: R.B.T.-S.A. Blackburn (Ed.), 5 - Sustainable dyeing technologies, Woodhead Publ. Ser. Text (2015) 135–160, https://doi.org/10.1016/B978-1-78242-339-3.00005-4.
[48] D. Nečas, P. Klapetek, Gwyddion: an open-source software for SPM data analysis, 10 (2012) 181–188. https://doi.org/10.2478/s11534-011-0096-2.
[49] L. Pei, H. Li, J. Shen, H. Zhang, J. Wang, Salt-free dyeing of cotton fabric and adsorption of reactive dyes in non-aqueous dyeing system: equilibrium, kinetics, and thermodynamics, Cellulose 29 (2022) 4753–4765. https://doi.org/10.1007/s10570-022-04576-9.
[50] Q. Hu, L. Pei, J. Shen, S. Sun, J. Wang, Level dyeing property and aggregation morphology of reactive black 5 on cotton fabric in a salt-free and less-water dyeing system, Text. Res. J. 94 (2023) 598–608, https://doi.org/10.1177/00405175231214191.
[51] A.M. Grancarić, A. Tarbuk, A. Sutlović, A. Castellano, C. Colleoni, G. Rosace, M. R. Plutino, Enhancement of acid dyestuff salt-free fixation by a cationizing sol-gel based coating for cotton fabric, Colloids Surfaces A Physicochem. Eng. Asp. 612 (2021) 125984, https://doi.org/10.1016/j.colsurfa.2020.125984.
[52] G. Brancatelli, C. Colleoni, M.R. Massafra, G. Rosace, Effect of hybrid phosphorus-doped silica thin films produced by sol-gel method on the thermal behavior of cotton fabrics, Polym. Degrad. Stab. 96 (2011) 483–490, https://doi.org/10.1016/j.polymdegradstab.2011.01.013.
[53] M. Pagliaro, R. Ciriminna, G. Palmisano, Silica-based hybrid coatings, J. Mater. Chem. 19 (2009) 3116–3126, https://doi.org/10.1039/B819615J.
[54] N. Yildirim, D. Odaci, G. Ozturk, S. Alp, Y. Ergun, K. Dornbusch, K.-H. Feller, S. Timur, Sol–gel encapsulated glucose oxidase arrays based on a pH sensitive fluorescent dye, Dye. Pigment. 89 (2011) 144–148, https://doi.org/10.1016/j.dyepig.2010.10.003.
[55] L. Gabrielli, L. Russo, A. Poveda, J.R. Jones, F. Nicotra, J. Jiménez-Barbero, L. Cipolla, Epoxide Opening versus Silica Condensation during Sol–Gel Hybrid Biomaterial Synthesis, Chem. – A Eur. J. 19 (2013) 7856–7864, https://doi.org/10.1002/chem.201204326.
[56] D. Carboni, A. Pinna, L. Malfatti, P. Innocenzi, Smart tailoring of the surface chemistry in GPTMS hybrid organic–inorganic films, New J. Chem. 38 (2014) 1635–1640, https://doi.org/10.1039/C3NJ01385E.
[57] L. Gabrielli, L. Connell, L. Russo, J. Jiménez-Barbero, F. Nicotra, L. Cipolla, J. R. Jones, Exploring GPTMS reactivity against simple nucleophiles: chemistry beyond hybrid materials fabrication, RSC Adv 4 (2014) 1841–1848, https://doi.org/10.1039/C3RA44748K.
[58] V. Trovato, A. Mezzi, M. Brucale, G. Rosace, M. Rosaria Plutino, Alizarin-functionalized organic-inorganic silane coatings for the development of wearable textile sensors, J. Colloid Interface Sci. 617 (2022) 463–477, https://doi.org/10.1016/j.jcis.2022.03.006.
[59] M.R. Plutino, C. Colleoni, I. Donelli, G. Freddi, E. Guido, O. Maschi, A. Mezzi, G. Rosace, Sol-gel 3-glycidoxypropyltriethoxysilane finishing on different fabrics: the role of precursor concentration and catalyst on the textile performances and cytotoxic activity, J. Colloid Interface Sci. 506 (2017) 504–517, https://doi.org/10.1016/j.jcis.2017.07.048.
[60] B.K.G. Theng, M. Russell, G.J. Churchman, R.L. Parfitt, Surface Properties of Allophane, Halloysite, and Imogolite, Clays Clay Miner 30 (1982) 143–149, https://doi.org/10.1346/CCMN.1982.0300209.
[61] G. Rosace, E. Guido, C. Colleoni, M. Brucale, E. Piperopoulos, C. Milone, M. R. Plutino, Halochromic resorufin-GPTMS hybrid sol-gel: chemical-physical properties and use as pH sensor fabric coating, Sensors Actuators, B Chem 241 (2017) 85–95, https://doi.org/10.1016/j.snb.2016.10.038.
[62] M. Amjadi, A. Samadi, J.L. Manzoori, A composite prepared from halloysite nanotubes and magnetite (Fe3O4) as a new magnetic sorbent for the preconcentration of cadmium(II) prior to its determination by flame atomic absorption spectrometry, Microchim. Acta 182 (2015) 1627–1633, https://doi.org/10.1007/s00604-015-1491-y.
[63] M. Krawczyk, S. Akbari, M. Jeszka-Skowron, E. Pajootan, F.S. Fard, Application of dendrimer modified halloysite nanotubes as a new sorbent for ultrasound-assisted dispersive micro-solid phase extraction and sequential determination of cadmium and lead in water samples, J. Anal. At. Spectrom. 31 (2016) 1505–1514, https://doi.org/10.1039/C6JA00096G.
[64] R. Li, Q. He, Z. Hu, S. Zhang, L. Zhang, X. Chang, Highly selective solid-phase extraction of trace Pd(II) by murexide functionalized halloysite nanotubes, Anal. Chim. Acta 713 (2012) 136–144, https://doi.org/10.1016/j.aca.2011.11.047.
[65] H. Zhu, M. Du, M. Zou, C. Xu, Y. Fu, Green synthesis of Au nanoparticles immobilized on halloysite nanotubes for surface-enhanced Raman scattering substrates, Dalt. Trans. 41 (2012) 10465–10471, https://doi.org/10.1039/C2DT30998J.
[66] S. Ranganatha, T.V. Venkatesha, Fabrication and electrochemical characterization of Zn–halloysite nanotubes composite coatings, RSC Adv 4 (2014) 31230–31238, https://doi.org/10.1039/C4RA02455A.
[67] P. Krishnaiah, C.T. Ratnam, S. Manickam, Development of silane grafted halloysite nanotube reinforced polylactide nanocomposites for the enhancement of mechanical, thermal and dynamic-mechanical properties, Appl. Clay Sci. 135 (2017) 583–595, https://doi.org/10.1016/j.clay.2016.10.046.
[68] X. Li, I. Nikiforow, K. Pohl, J. Adams, D. Johannsmann, Polyurethane Coatings Reinforced by Halloysite Nanotubes, Coatings 3 (2013) 16–25, https://doi.org/10.3390/coatings3010016.
[69] P. Sun, G. Liu, D. Lv, X. Dong, J. Wu, D. Wang, Effective activation of halloysite nanotubes by piranha solution for amine modification via silane coupling chemistry, RSC Adv 5 (2015) 52916–52925, https://doi.org/10.1039/C5RA04444H.
[70] Y. He, W. Xu, R. Tang, C. Zhang, Q. Yang, pH-Responsive nanovalves based on encapsulated halloysite for the controlled release of a corrosion inhibitor in epoxy coating, RSC Adv 5 (2015) 90609–90620, https://doi.org/10.1039/C5RA19296J.
[71] M. Raji, M.E.M. Mekhzoum, D. Rodrigue, A. el kacem Qaiss, R. Bouhfid, Effect of silane functionalization on properties of polypropylene/clay nanocomposites, Compos. Part B Eng. 146 (2018) 106–115, https://doi.org/10.1016/j.compositesb.2018.04.013.
[72] K. Fang, C. Zhang, Surface physical–morphological and chemical changes leading to performance enhancement of atmospheric pressure plasma treated polyester fabrics for inkjet printing, Appl. Surf. Sci. 255 (2009) 7561–7567, https://doi.org/10.1016/j.apsusc.2009.04.028.